

Dual-band Antenna Feed Solution for 5G

A dual-band coaxial- and waveguide fed antenna feed for reflector antenna systems

Master's thesis in Wireless, photonics and space engineering

LUKAS MARED

MASTER'S THESIS 2018:NN

Dual-band Antenna Feed Solution for 5G

A dual-band coaxial- and waveguide fed antenna feed for reflector
antenna systems

LUKAS MARED



CHALMERS
UNIVERSITY OF TECHNOLOGY

Department of Electrical Engineering
Division of Communication and Antenna Systems
Antenna Systems Group
CHALMERS UNIVERSITY OF TECHNOLOGY
Gothenburg, Sweden 2018

Dual-band Antenna Feed Solution for 5G
A dual-band coaxial- and waveguide fed antenna feed for reflector antenna systems
LUKAS MARED

© LUKAS MARED, 2018.

Supervisor: Tomas Östling, CTO, LEAX Arkivator Telecom AB
Supervisor: Thomas Schäfer, Antenna Engineer, LEAX Arkivator Telecom AB
Supervisor: Ashraf Uz Zaman, Assistant Professor, Department of Electrical Engineering
Examiner: Jian Yang, Professor, Department of Electrical Engineering

Master's Thesis 2018:NN
Department of Electrical Engineering
Division of Communication and Antenna Systems
Antenna Systems Group
Chalmers University of Technology
SE-412 96 Gothenburg
Telephone +46 31 772 1000

Cover: The final design of the antenna feed with the sub-reflector.

Typeset in L^AT_EX
Printed by [Name of printing company]
Gothenburg, Sweden 2018

Dual-band Antenna Feed Solution for 5G

A dual-band coaxial- and waveguide fed antenna feed for reflector antenna systems
LUKAS MARED

Department of Electrical Engineering
Chalmers University of Technology

Abstract

Antenna feeds for sub reflectors are a key component in backhaul. For the evolving 5G the data rates need to be higher, and a higher frequency band has been allocated for this intercommunication. This band needs to be efficiently incorporated with the previously allocated, lower frequency band, to utilize a dual band setup for the base station intercommunication.

In this thesis project two different concepts for a dual-band dual-polarized antenna feed solution for reflector antenna systems was investigated. The two bands investigated are K_u-K (17.7-19.7 GHz) and E-band (71-76, and 81-86 GHz).

The first concept is a ridged waveguide coaxial- and waveguide fed feed. The resulting reflection coefficient for the system was better than -11.5 dB for the lower band, and better than -6 dB for the upper band. The far field characteristics was not investigated for this concept.

The second concept is a single-polarized coaxial- and waveguide fed feed using a pin-structure as backshort for the coaxial feed. The resulting reflection coefficient was better than -24dB for the lower band, and better than -24dB for the upper band, without the sub reflector. With the unoptimized sub reflector the result is better than -11 dB and -6dB respectively. The aperture efficiency for the lower band is better than 65% and better than 15% for the upper band. The low aperture efficiency for the higher band is due to poor phase efficiency. The second concept is to be manufactured and measured upon.

Keywords: ridged, waveguide, dual, band, polarized, coaxial, feed, antenna.

Acknowledgements

This thesis project was carried out at Chalmers University of Technology at the antenna group, for LEAX Arkivator Telecom AB, together with Thomas Schäfer (LEAX), Tomas Östling (LEAX), Ashraf Uz Zaman (Chalmers), and Jian Yang (Chalmers).

I would like to especially thank Thomas and Ashraf for their great assistance during my thesis work. I would also like to thank Tomas and Jian for their brilliant ideas which made this thesis work possible.

I am also very grateful towards the help from the mechanical and antenna engineers at LEAX who have helped me during the design- and manufacturing process.

Lukas Mared, Gothenburg, June 2018

Contents

List of Figures	xi
List of Tables	xv
1 Introduction	1
1.1 Aim of the project	1
1.2 Demarcation	1
2 Theory	3
2.1 Waveguide theory	3
2.1.1 Rectangular waveguide	3
2.1.2 Circular waveguide	4
2.1.3 Higher order modes	6
2.1.4 Periodic reflections	7
2.1.5 Ridge design	7
2.2 Antenna theory	8
2.2.1 Field theory	9
2.2.2 Polarization	9
2.2.2.1 Co-polar and cross-polar	10
2.2.3 Paraboloid reflector antenna	11
2.2.4 Subreflector	11
2.2.4.1 Efficiencies	12
2.3 Excitation	13
2.3.1 Waveguide excitation	14
2.3.2 Coaxial feed excitation	14
3 Design and manufacturing of the feed	17
3.1 Design of E-band feed and waveguide	17
3.1.1 E-band waveguide transition	17
3.2 Design of 18 GHz-band excitation	21
3.2.1 Coaxial feed with ridges	21
3.2.1.1 Ridge design	21
3.2.1.2 E-band performance	23
3.2.2 Coaxial feed without ridges	25
3.2.2.1 Pin structure design	26
3.2.2.2 E-band performance	29
3.3 Manufacturing	30

3.3.1	E-band transition	30
3.3.2	18 GHz excitation	30
3.3.2.1	Pin structure	31
3.3.3	Finalized structure	31
4	Results	33
4.1	18 GHz band	34
4.1.1	Far field results	36
4.2	E-band	45
4.2.1	Farfield results	46
5	Discussion and further work	57
5.1	Dual-band antenna feed	57
5.2	Ridge design	57
5.3	Pin structure design	57
5.4	Results	58
5.4.1	Efficiencies	58
5.5	Future work	58
	Bibliography	59
A	Appendix 1	I

List of Figures

2.1	Standardized dimensions of a rectangular waveguide along with the fundamental mode distribution.	4
2.2	Standardized dimensions of a circular waveguide seen from a cross-sectional cut.	5
2.3	The first six solutions for modes in a circular waveguide, starting from top left, moving to the right: The TE_{11} , TM_{01} , TE_{21} , TE_{01} , TM_{11} , and finally TE_{31}	6
2.4	Cut-off properties for alternating ridge dimensions in a circular waveguide with a nominal cut-off frequency of 55.32 GHz.	8
2.5	A circular waveguide setup with ridges for one polarization.	8
2.6	A 45° x- and y-polarized signal propagating in z-direction.	9
2.7	Top left shows an x-polarized signal, top right a y-polarized signal, bottom left a right-handed circularly polarized signal, and bottom right left-handed circularly polarized signal. The propagation direction is in +z-direction.	10
2.8	The hat feed divided in to three main components. "1" is the hat, "2" is the head, and "3" is the neck.	12
2.9	The subtended angle θ of a parabolic reflector with a subreflector.	13
2.10	Visualization of a coaxial feed in an ideal waveguide.	14
3.1	Two cubic Bézier curves with different defining points. The dashed lines represent the lines between each point, and the lines the resulting Bézier curves.	19
3.2	Visualization of the optimized E-band transition with a Bézier profile.	20
3.3	The reflection coefficient for the feed after optimization.	20
3.4	The transmission coefficient for the feed after optimization.	20
3.5	An explanation of the mathematical curve used for the ridge design. O is the ridge opening, R shows two different opening rates, where the dotted one has a higher opening rate, and L shows the length of the ridges.	22
3.6	The optimized structure with ridges and coaxial feed.	22
3.7	The resulting reflection coefficient of the coaxial feed in the optimized structure with ridges.	23
3.8	The resulting reflection coefficient seen from the E-band port in the optimized structure with ridges.	23

3.9	The resulting transmission coefficient between the E-band ports in the optimized structure with ridges.	24
3.10	The resulting reflection coefficient between at the E-band port with ridges optimized for E-band.	24
3.11	The resulting transmission coefficient between the E-band ports with ridges optimized for E-band.	25
3.12	A schematic figure showing the setup of the pin structure concept, which acts as a single-polarized electrical wall.	26
3.13	A schematic figure showing the parameters that were optimized for in order to improve results. "a" is the pin displacement, "b" is the relative distance between the pin wall and coaxial feed. "c" is the insert length of the coaxial conductor, "d" is the offset from the end of the transition, and e is the insert length of the coaxial dielectric. The thickness of the pins is the width in x-direction, and length is the width in y-direction.	27
3.14	The reflection coefficient for different pin displacement around 18 GHz.	27
3.15	The reflection coefficient for different pin setups.	28
3.16	The reflection coefficient for different pin geometry setups. For all cases the coaxial conductor insert is 3.3mm, the dielectric insert is 0mm, the distance between the pin wall and conductor is 5.9mm and the thickness is 0.2mm. For the sheet-case the length of the pins are 1mm.	29
3.17	The reflection coefficient for different pin geometries at E-band.	29
3.18	The reflection coefficient for different pin thicknesses at E-band	30
3.19	A schematic figure showing the new design. The sections "a", "b", and "c" are manufactured in three separate processes. The E-band port is the leftmost part, i.e. start of "a".	31
3.20	The mechanical design of the antenna feed. The sections "a", "b", and "c" are manufactured in three separate processes. Section "d" is the rectangular to circular transition obtained by LEAX Arkivator Telecom AB.	32
3.21	The mechanical design of the antenna feed. The sections "a", "b", and "c" are manufactured in three separate processes. Section "d" is the rectangular to circular transition obtained by LEAX Arkivator Telecom AB.	32
4.1	The finalized structure simulated in CST without the sub reflector.	33
4.2	The finalized structure simulated in CST with the sub reflector.	34
4.3	The simulated reflection coefficient for the 18 GHz-band port to port simulation	35
4.4	The simulated reflection coefficients for the 18 GHz-band horn antenna simulation with and without sub reflector.	35
4.5	Farfield plot of the antenna feed at 17.7 GHz	36
4.6	3D Farfield plot of the H-plane of the antenna feed at 17.7 GHz	37
4.7	3D Farfield plot of the E-plane of the antenna feed at 17.7 GHz	37
4.8	Farfield plot of the antenna feed at 18.7 GHz	38

4.9	3D Farfield plot of the H-plane of the antenna feed at 18.7 GHz . . .	38
4.10	3D Farfield plot of the E-plane of the antenna feed at 18.7 GHz . . .	39
4.11	Farfield plot of the antenna feed at 19.7 GHz	39
4.12	3D Farfield plot of the H-plane of the antenna feed at 19.7 GHz . . .	40
4.13	3D Farfield plot of the E-plane of the antenna feed at 19.7 GHz . . .	40
4.14	Farfield plot of the antenna feed with the sub reflector at 17.7 GHz. The angle is reversed, and 180 degrees is forward.	41
4.15	3D Farfield plot of the H-plane of the antenna feed with the sub reflector at 17.7 GHz	41
4.16	3D Farfield plot of the E-plane of the antenna feed with the sub reflector at 17.7 GHz	42
4.17	Farfield plot of the antenna feed with the sub reflector at 18.7 GHz. The angle is reversed, and 180 degrees is forward.	42
4.18	3D Farfield plot of the H-plane of the antenna feed with the sub reflector at 18.7 GHz	43
4.19	3D Farfield plot of the E-plane of the antenna feed with the sub reflector at 18.7 GHz	43
4.20	Farfield plot of the antenna feed with the sub reflector at 19.7 GHz. The angle is reversed, and 180 degrees is forward.	44
4.21	3D Farfield plot of the H-plane of the antenna feed with the sub reflector at 19.7 GHz	44
4.22	3D Farfield plot of the E-plane of the antenna feed with the sub reflector at 19.7 GHz	45
4.23	The simulated reflection coefficients for the E-band port to port sim- ulation.	45
4.24	The simulated reflection coefficients for the E-band horn antenna sim- ulation with and without sub reflector.	46
4.25	Farfield plot of the antenna feed at 71 GHz	47
4.26	3D Farfield plot of the E-plane of the antenna feed at 71 GHz	47
4.27	3D Farfield plot of the H-plane of the antenna feed at 71 GHz	48
4.28	Farfield plot of the antenna feed at 78.5 GHz	48
4.29	3D Farfield plot of the E-plane of the antenna feed at 78.5 GHz . . .	49
4.30	3D Farfield plot of the H-plane of the antenna feed at 78.5 GHz . . .	49
4.31	Farfield plot of the antenna feed at 86 GHz	50
4.32	3D Farfield plot of the E-plane of the antenna feed at 86 GHz	50
4.33	3D Farfield plot of the H-plane of the antenna feed at 86 GHz	51
4.34	Farfield plot of the antenna feed with the sub reflector at 71 GHz. The angle is reversed, and 180 degrees is forward.	51
4.35	3D Farfield plot of the E-plane of the antenna feed with the sub reflector at 71 GHz	52
4.36	3D Farfield plot of the H-plane of the antenna feed with the sub reflector at 71 GHz	52
4.37	Farfield plot of the antenna feed with the sub reflector at 78.5 GHz. The angle is reversed, and 180 degrees is forward.	53
4.38	3D Farfield plot of the E-plane of the antenna feed with the sub reflector at 78.5	53

4.39	3D Farfield plot of the H-plane of the antenna feed with the sub reflector at 78.5	54
4.40	Farfield plot of the antenna feed with the sub reflector at 86 GHz. The angle is reversed, and 180 degrees is forward.	54
4.41	3D Farfield plot of the E-plane of the antenna feed with the sub reflector at 86 GHz	55
4.42	3D Farfield plot of the E-plane of the antenna feed with the sub reflector at 86 GHz	55

List of Tables

2.1	The first nine solutions of the second-order differential Bessel equation for transverse electrical modes of a circular waveguide [2].	5
2.2	The first nine solutions of the second-order differential Bessel equation for transverse magnetic modes of a circular waveguide [2].	5
4.1	The efficiencies for the simulated antenna feed with sub reflector. . .	36
4.2	The efficiencies for the simulated antenna feed with sub reflector. . .	46

1

Introduction

Base station to base station communication is key in telecommunication. Previously this has been done in different ways, through fiber, a point-to-point connection, et.c.. The point-link connection has been limited to a frequency of 17.7 to 19.7 GHz. However, there is a need to increase the bandwidth of the point-link connection due to the development of 5G, and now a part of the E-band has been allocated for this use, more specifically 71 to 76 and 81 to 86 GHz. Higher frequencies does not only have the benefits of increased bandwidth. Generally with a higher frequency there is a higher attenuation over distance, and may be highly dependant on weather conditions, such as rain. Due to this the transition to only use E-band in point-link communication may not be feasible. Thus there is a need to effectively combine the lower frequency band (17.7 to 19.7 GHz), with the higher, more newly allocated E-band. This can be done with an antenna transmitting and receiving signals at two different polarizations. This report covers the investigation, design, optimization, and manufacturing of a dual-band antenna feed which can transmit and receive both the upper and lower band of requirement, at different polarizations.

1.1 Aim of the project

The aim of the project is to investigate the performance, design limitations and viability of a dual-band dual-polarized antenna feed. At the time of the project very few dual-band dual-polarized feeds have been designed and manufactured and therefore there will be no requirement on performance. This project will rather focus on investigating how well a dual-band dual-polarized antenna feed design can perform.

1.2 Demarcation

The design process does not investigate or analyze the possibility to use an ortho-mode transducer (OMT) as the feed for the lower frequency band. The feed geometry is limited to a circular waveguide design, and a square waveguide is not investigated.

The coaxial cables used in this design are off-the-shelf, and optimized conductor and dielectric radius are not included in the design process. Lastly, the waveguide ports used are standardized dimensions used by LEAX Arkivator Telecom AB, and are not optimized as a part of this design. These demarcations were made because of limitations in time.

2

Theory

2.1 Waveguide theory

A waveguide is a structure which guides electromagnetic waves, which enables low-loss propagation at high frequencies and is a key component in many microwave applications. These waveguides can consist of many different shapes and sizes, but most commonly it is a hollow metallic structure such as rectangular, circular or elliptical. These types of waveguides support transverse electric (TE) or transverse magnetic (TM) modes, i.e. a mode which either has a magnetic or electric longitudinal component. Rectangular and circular are two of the most commonly used waveguides and have both their advantages and disadvantages. The rectangular waveguide is simpler to excite, whereas the circular waveguide introduces lower loss [1]. Waveguides, however, has a certain cut-off frequency depending on the dimensions of the waveguide, and a signal with a frequency lower than the cut-off can not propagate through the structure. This cut-off frequency depends on the shape of the waveguide, which will be explained more explicitly below.

The main part of this project is the design of a waveguide antenna feed for a parabolic reflector antenna, where the most commonly used shapes are rectangular and circular waveguides. The theory of these waveguides will be provided below.

2.1.1 Rectangular waveguide

The rectangular waveguide is used mostly thanks to its simplicity to excite and design. A cross-sectional cut of a rectangular waveguide can be seen in figure 2.1.

As mentioned previously a waveguide has a cut-off frequency depending on the dimensions and can be formulated as follows [2]:

$$f_{c,mn} = \frac{1}{2\pi\sqrt{\mu\epsilon}} \sqrt{\left(\frac{m\pi}{a}\right)^2 + \left(\frac{n\pi}{b}\right)^2} \quad (2.1)$$

Where a and b are the dimensions of the waveguide which can be seen in figure 2.1, along with the fundamental mode distribution

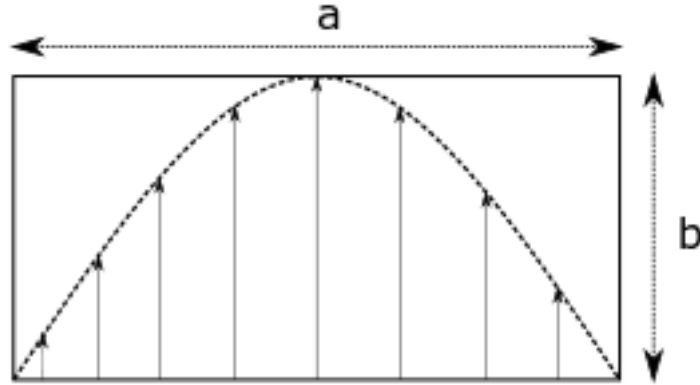


Figure 2.1: Standardized dimensions of a rectangular waveguide along with the fundamental mode distribution.

and μ and ϵ is the permeability and permittivity inside the waveguide respectively. A waveguide can only sustain an integer number of modes (0, 1,..), and these are represented by the terms m and n in the equation. As such, it can be seen that the first propagating mode in a rectangular waveguide with dimensions as the one in the figure, is the TE_{10} mode, since $a > b$. Thus the cut-off frequency for the first propagating mode in this waveguide is:

$$f_{c,10} = \frac{1}{2a\sqrt{\mu\epsilon}} \quad (2.2)$$

If the waveguide is assumed to be hollow and contain only vacuum the equation can be rewritten:

$$f_{c,10} = \frac{c}{2a} \quad (2.3)$$

Where c is the speed of light. Since the wavelength is defined as the speed of light divided by the frequency of the wave the equation can be rewritten once more:

$$a = \frac{\lambda_{c,10}}{2} \quad (2.4)$$

As such it can be seen that the first propagating wave will occur when the rectangular waveguide has one of its sides (a or b) equal to half a wavelength. Higher-order modes will be generated at multiples of this value for the rectangular waveguide case.

2.1.2 Circular waveguide

The circular waveguide is, similarly to the rectangular waveguide, a simple design. However, the circular waveguide is more difficult to excite, especially in applications where control of the polarization is needed. An advantage with the circular waveguide is that it has lower loss than the rectangular waveguide and the fundamental mode has a polarization angle which can be used for different applications. A cross-sectional cut of a circular waveguide can be seen in figure 2.2

n	p'_{n1}	p'_{n2}	p'_{n3}
0	3.832	7.016	10.174
1	1.841	5.331	8.536
2	3.054	6.706	9.970

Table 2.1: The first nine solutions of the second-order differential Bessel equation for transverse electrical modes of a circular waveguide [2].

n	p_{n1}	p_{n2}	p_{n3}
0	2.405	5.520	8.654
1	3.832	7.016	10.174
2	5.135	8.417	11.620

Table 2.2: The first nine solutions of the second-order differential Bessel equation for transverse magnetic modes of a circular waveguide [2].

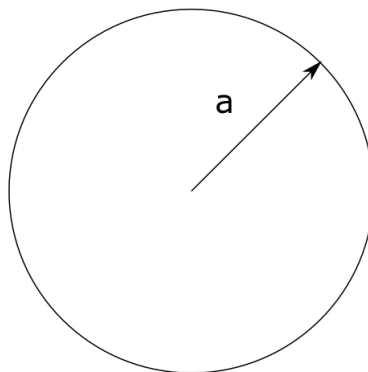


Figure 2.2: Standardized dimensions of a circular waveguide seen from a cross-sectional cut.

The cut-off frequency for a circular waveguide can be expressed accordingly:

$$f_{c,mn} = \frac{p'_{mn}}{2\pi a \sqrt{\mu\epsilon}} \quad (2.5)$$

Where a , as can be seen in the figure, is the radius from the center of the circle, μ and ϵ is the permeability and permittivity respectively. p'_{mn} is a solution to the second-order differential Bessel equation, and determines which mode that propagates. This is different from the rectangular waveguide case as this is not an integer solution. However, it still only supports an integer number of modes. The solutions to the first nine TE and TM modes can be seen in the tables 2.1, and 2.2 [2].

The fundamental mode for a circular waveguide, the TE_{11} mode, is not circularly symmetric, i.e. it has a polarization. As such, if the waveguide is excited such that it contains two orthogonal modes, these two modes can transmit energy and

propagate independently from each other and thereby double the amount of data sent compared to one polarization. The TE_{11} mode field distribution, along with a few other mode field distributions, can be seen in figure 2.3 [2].

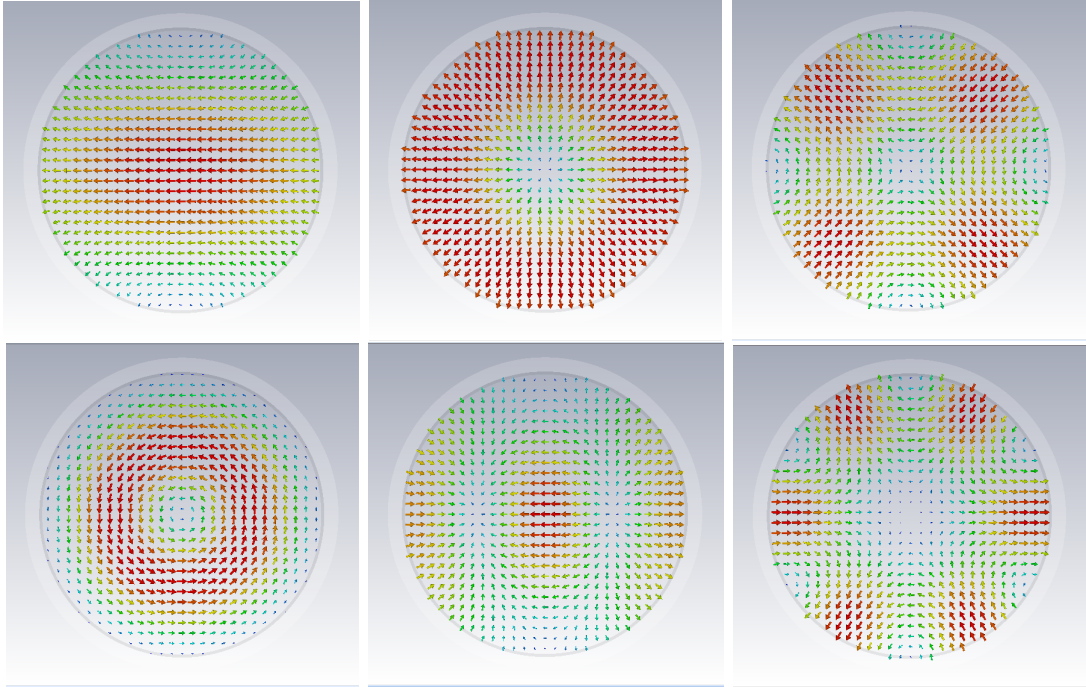


Figure 2.3: The first six solutions for modes in a circular waveguide, starting from top left, moving to the right: The TE_{11} , TM_{01} , TE_{21} , TE_{01} , TM_{11} , and finally TE_{31} .

Thus the exciting of the circular waveguide is of utmost importance to achieve optimum performance of the waveguide, and small polarization errors in the signal can destructively interfere with the other orthogonally polarized signal and thus decrease the performance.

2.1.3 Higher order modes

As was mentioned previously, the generation of higher order modes can occur in a waveguide. These can be generated when the waveguide's size is large enough to sustain more modes than the fundamental, i.e. in the rectangular case, the second order mode can propagate when a equals one wavelength. When a higher order mode is generated the field structure inside the waveguide differs to that from the fundamental mode case. This can cause problems in many applications, e.g. where the signal is used for data-transmission and the signal is modulated. This thus creates problems when there is a need to transmit two signals at different bands throughout the same waveguide structure. Transmitting a signal at E-band and 18 GHz simultaneously through a circular waveguide will thus mean that the E-band signal may contain more than 20 different modes. There are some ways to alter the design of the waveguide in order to increase the cut-off frequency for the higher order modes, or to lower the cut-off frequency of the fundamental mode. One

example which utilizes the second property will be explained more in detail in a ridged waveguide.

2.1.4 Periodic reflections

When designing antennas the waveguide impedance needs to be properly matched to the port. When there is a mismatch a portion of the energy in the wave will be reflected back resulting in a lower transmission. Especially when designing transitions there may be several interfaces where there is a mismatch, thus resulting in multiple reflections. These reflections may interfere with each other and a higher portion of the energy will be reflected at distinct frequencies. To find these frequencies, assume the following case: Two mismatches are positioned at z_1 and z_2 , and have reflection coefficients r_1 and r_2 . The total reflection is then:

$$|r| = |r_1 + r_2 e^{-j2\beta(z_2 - z_1)}| \quad (2.6)$$

However, the propagation constant β is a 2π periodic function and thus r is as well. To find the periodicity of the frequency for the reflections the phase term can be analyzed more carefully:

$$2\beta_1(z_2 - z_1) - 2\beta_2(z_2 - z_1) = 2\pi \implies \beta_2 - \beta_1 = \frac{\pi}{(z_2 - z_1)} \quad (2.7)$$

Which can then be reformulated to the following equation using $\beta = 2\pi/\lambda$:

$$\Delta f = \frac{c}{2(z_2 - z_1)} \quad (2.8)$$

This implies that if there are more than one mismatches in the structure there will be periodic reflections. This will increase the total energy reflected of the system at certain frequencies compared to a single mismatch. [3]

2.1.5 Ridge design

By using ridges inside the waveguide it is possible to decrease the cut-off frequency of the fundamental mode of the waveguide. According to [13] there is a possibility to lower the cut-off by at least a factor of 3.7. The cut-off frequency for different ridge openings and widths has been calculated in Computer Simulation Technology Microwave Studios (CST MWS) which is a simulation software for high frequency applications, and can be visualized in figure 2.4, and the waveguide setup with ridges can be visualized in figure 2.5.

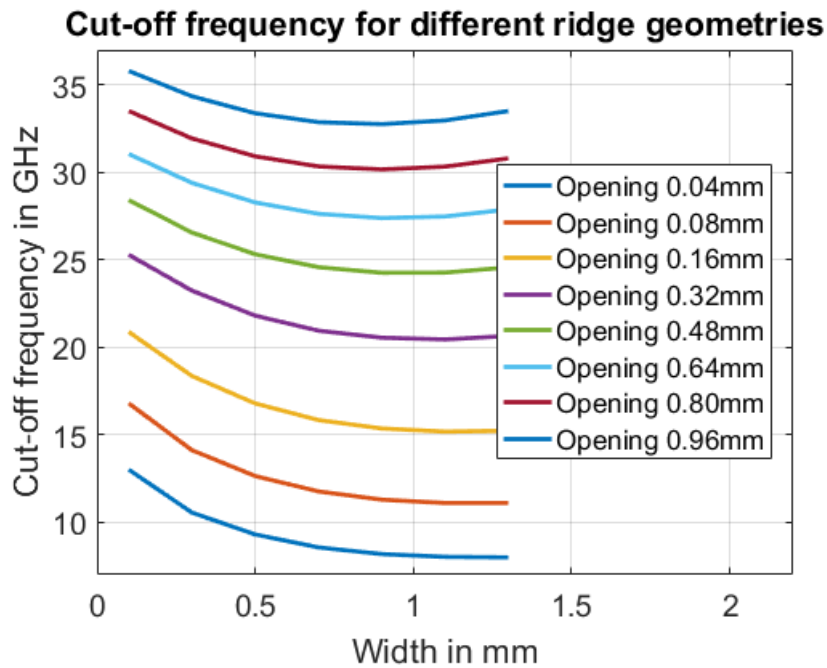


Figure 2.4: Cut-off properties for alternating ridge dimensions in a circular waveguide with a nominal cut-off frequency of 55.32 GHz.

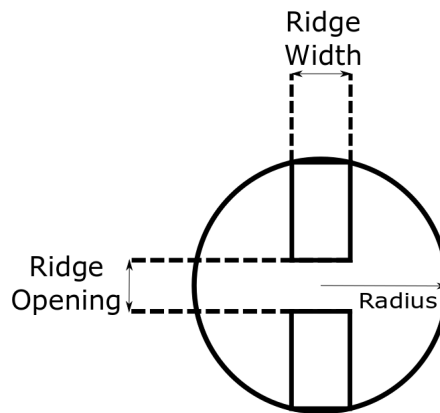


Figure 2.5: A circular waveguide setup with ridges for one polarization.

Thus a visual analysis of the figure shows that there is a theoretical possibility to lower the cut-off frequency from 55.3 GHz to 8 GHz, i.e. a factor of almost 7.

2.2 Antenna theory

This section will provide some fundamental antenna theory necessary for understanding the report.

2.2.1 Field theory

Electromagnetic fields and signals are characterized by vectoral fields, which propagate in a certain direction. These fields are normally described as instantaneous or time-harmonic fields [3].

$$\vec{E}(x, y, z, t) = \Re\{\mathbf{E}(x, y, z)e^{j\omega t}\} \quad (2.9)$$

Where \vec{E} is the instantaneous field, and \mathbf{E} is the time-harmonic field. The time-harmonic field can also be described accordingly if considered to be a plane wave propagating in free space in z-direction:

$$\mathbf{E} = \mathbf{E}_t e^{-jkz} = [E_x \hat{\mathbf{x}} + E_y \hat{\mathbf{y}}] e^{-jkz} \quad (2.10)$$

The magnetic field is described by

$$\mathbf{H} = \frac{1}{\eta} \hat{\mathbf{z}} \times \mathbf{E} \quad (2.11)$$

Where η is the free space wave impedance, which equals $120\pi \Omega$. k is the wave number,

$$k = \frac{2\pi}{\lambda} \quad (2.12)$$

and λ is the free-space wavelength.

2.2.2 Polarization

As could be seen in the previous chapter the electrical and magnetic fields is characterized by vector fields which describe the direction of the energy in the field. The direction the energy of the field is pointing in over a period of the wave is often called the polarization. This can be more easily understood if the previous equations are rewritten in the following form:

$$\Re\{\mathbf{E}e^{-j\omega t}\} = \Re\{[E_x \hat{\mathbf{x}} + E_y \hat{\mathbf{y}}]e^{-j\omega t}\} = E_x \hat{\mathbf{x}} \cos(\omega t - kz) + E_y \hat{\mathbf{y}} \cos(\omega t - kz) \quad (2.13)$$

Assuming that $E_x = E_y$ the following field is generated:

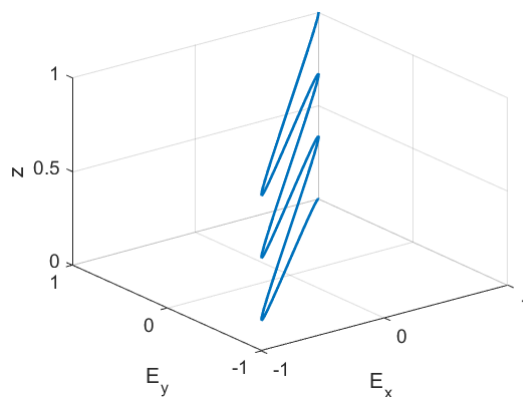


Figure 2.6: A 45° x- and y-polarized signal propagating in z-direction.

The most common signal polarizations are linearly polarized, e.g. x- or y-polarization, or right-handed circularly polarized (RHCP) or left-handed circularly polarized (LHCP) signals. x- or y-polarized signals occur when either E_x or E_y equals 0 respectively. RHCP occur when E_y is phase-delayed by 90° relative to E_x , and LHCP vice versa. These different polarizations can be seen in figure 2.7.

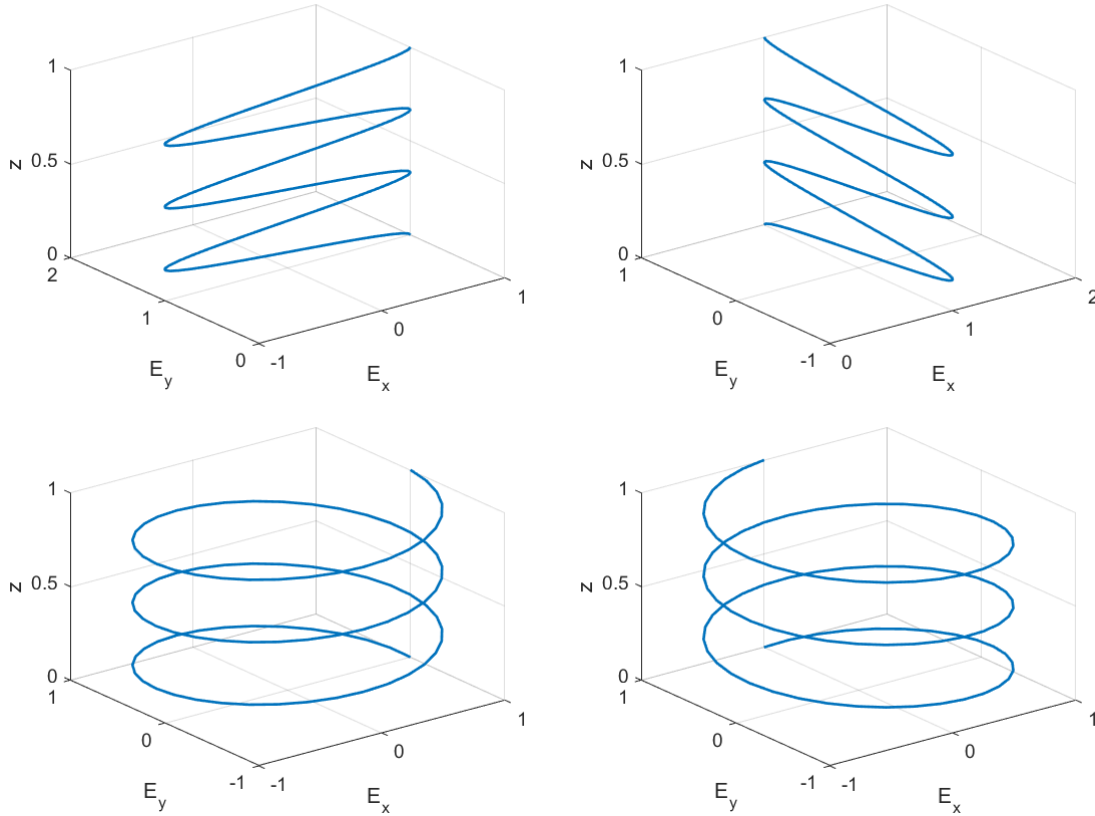


Figure 2.7: Top left shows an x-polarized signal, top right a y-polarized signal, bottom left a right-handed circularly polarized signal, and bottom right left-handed circularly polarized signal. The propagation direction is in $+z$ -direction.

By transmitting signals at different polarizations there is a possibility to transmit two different signals at the same frequency from the same antenna simultaneously, since two orthogonally polarized signals will not interfere with one another.

2.2.2.1 Co-polar and cross-polar

Since the polarization of a signal can be desired to be different for different applications, there is a convention which simplifies the description of which polarization is the desired and undesired one. This is usually said to be the "co-polar" polarization component, and "cross-polar" polarization component, where the co-polar component is the desired one, and the cross-polar component is the undesired one. These are defined as two general orthogonally polarized signals, i.e.

$$\hat{\mathbf{c}}\mathbf{o} \cdot \hat{\mathbf{c}}\mathbf{o}^* = 1, \quad \hat{\mathbf{c}}\mathbf{o} \cdot \hat{\mathbf{x}}\mathbf{p}^* = 0 \quad (2.14)$$

$$\hat{\mathbf{x}}\hat{\mathbf{p}} \cdot \hat{\mathbf{x}}\hat{\mathbf{p}}^* = 1, \quad \hat{\mathbf{x}}\hat{\mathbf{p}} \cdot \hat{\mathbf{c}}\hat{\mathbf{o}}^* = 0 \quad (2.15)$$

Thus to find the desired polarization of the signal the electric field should be scalar multiplied with the co-polar component, and similarly for the undesired, but with the cross-polar component.

If the desired polarization is e.g. x-polarization the co polarization can be found accordingly:

$$\hat{\mathbf{c}}\hat{\mathbf{o}} = \hat{\mathbf{x}} = \cos \varphi \hat{\boldsymbol{\theta}} - \sin \varphi \hat{\boldsymbol{\phi}} \quad (2.16)$$

2.2.3 Paraboloid reflector antenna

The paraboloid reflector antenna focuses and directs the power transmitted in a small pencil-like beam which has a high directivity. The directivity of the antenna is (roughly) proportional to the diameter of the parabolic reflector, and the beamwidth is inversely proportional to the diameter. [3] The entire paraboloid antenna reflector system can consist of many different parts, but these are commonly divided in three different components: The parabolic reflector, the subreflector, as well as the antenna feed. The characterization of the performance of the antenna feed and sub-reflector components are usually measured in efficiencies [3]. These efficiencies, as well as the subreflector will be explained more in detail in the following sections.

2.2.4 Subreflector

A well-known and commonly used paraboloid reflector antenna system is the so called hat-fed reflector antenna which relies on a self supported rear-radiating sub-reflector and antenna feed combination. A major benefit of this system is that there is no need for supporting structures as both the subreflector and antenna feed are integrated in one another, and is a central part of the reflector antenna system. It was firstly introduced by Kildal [4].

The hat feed itself is divided in three components, the neck, the head, and the hat, see figure 2.8:

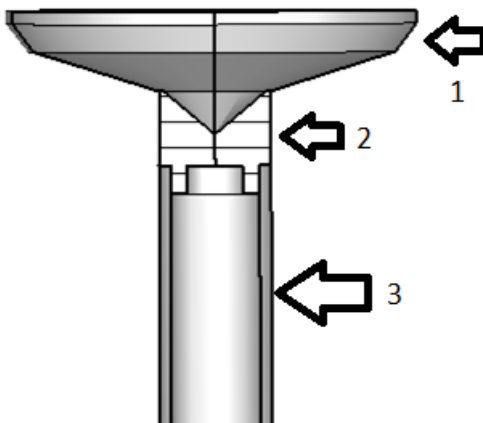


Figure 2.8: The hat feed divided in to three main components. "1" is the hat, "2" is the head, and "3" is the neck.

The neck is the waveguide feed used to feed the reflector antenna system. The head is a supporting structure which holds the hat, which usually is a dielectric structure. However, there are examples of heads not using any dielectric support structure [5]. Lastly there is the hat which (in this example) consists of a reflecting circular crown structure with an angular profile which is optimized for illuminating the parabolic reflector. The size and angular profile of the hat is optimized for the parabolic reflector dimensions and frequency of operation. It is also common for the hat to be corrugated [4].

The market uses for the hat feed are e.g. satellite communication systems [6] and telecommunication backhaul.

2.2.4.1 Efficiencies

The efficiencies used to characterize the performance are divided up in to four different parts, the spillover, polarization, illumination and phase efficiency [3]:

$$e_{ap} = e_{sp}e_{pol}e_{ill}e_{\phi} \quad (2.17)$$

Three of these can be analysed and calculated from the antenna feed by analysing it as a horn antenna, given that the subtended angle is known, i.e. the angle from the sub-reflector relative the parabolic dish, see figure 2.9.

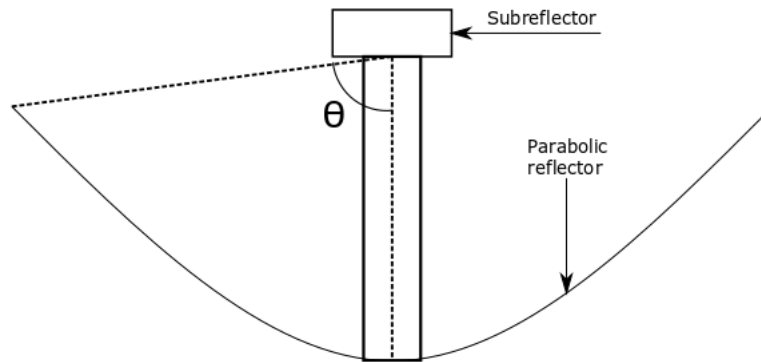


Figure 2.9: The subtended angle θ of a parabolic reflector with a subreflector.

These are the spillover efficiency, the polarization efficiency and the phase efficiency. To analyse the illumination efficiency the performance of the sub-reflector needs to be known as well. These three efficiencies are thus key for designing an antenna feed.

Spillover efficiency e_{sp} The spillover efficiency is the amount of power illuminating the reflector relative to the total amount of power transmitted by the feed. (i.e. the power within the subtended angle relative the total power transmitted).

Polarization efficiency e_{pol} This is the power of the co-polar field relative to the total amount of power within the subtended angle (i.e. the amount of wanted polarization illuminating the reflector relative to the total power illuminating the reflector).

Illumination efficiency e_{ill} Illumination efficiency is a measurement of how well the reflector is illuminated, i.e. how big portion of the aperture is efficiently used. If the entire aperture is uniformly illuminated this efficiency is 100%. However, the aperture is normally illuminated less at higher angles to e.g. reduce the spillover. To evaluate this efficiency the far-field of the feed with the subreflector needs to be known, since the subreflector will impact the field incident on the reflector.

Phase efficiency e_{ϕ} In order to maximize the gain from an antenna, the phase over the whole aperture should be constant. The phase efficiency is a measurement of the phase error of the far field from the feed, i.e. the "evenness" of the phase over the antenna aperture. If the phase center is not properly placed destructive interference may occur and the performance will decrease.

2.3 Excitation

This section will provide explanation of two common procedures of exciting a waveguide.

2.3.1 Waveguide excitation

A common way is to excite the waveguide with another waveguide connected to a signal generator. This waveguide is commonly of a rectangular shape.

2.3.2 Coaxial feed excitation

Exciting circular waveguides with coaxial feeds is a common occurrence. There are many off-the-shelf solutions for this and a common way is to excite inserting the probe in to the structure with a backshort placed approximately a quarter-wavelength back, see figure 2.10

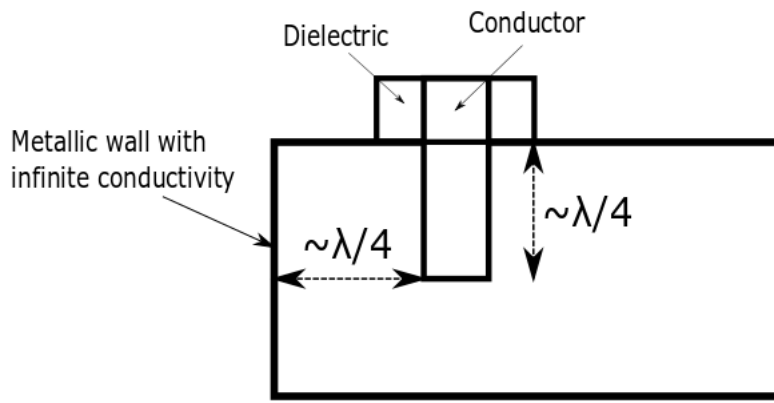


Figure 2.10: Visualization of a coaxial feed in an ideal waveguide.

These feeds can commonly achieve a very good return loss (up to -30dB over a large frequency range) [11]. The polarization of the signal is also in the direction of insertion of the conductor, i.e. it is linearly polarized in the direction of the conductor. The reason for locating the feed a quarter-wavelength in front of the wall is to utilize the reflection and have a standing waveguide pattern constructively interfering with the electrical signal excited from the coaxial feed. However, due to the properties of the waveguide the wavelength inside a waveguide is not equal to that of free-space, it is slightly longer, as the wavelength is proportional to the propagation constant [2]:

$$\lambda_g = \frac{2\pi}{\beta} \quad (2.18)$$

and the propagation constant is proportional to the cut-off properties of the waveguide:

$$\beta = \sqrt{k^2 - k_c^2} \quad (2.19)$$

Where k_c is the cut-off wavenumber which equals

$$k_c = \begin{cases} \sqrt{(m\pi/a)^2 + (n\pi/b)^2} & \text{for a rectangular waveguide} \\ \frac{p'_{nm}}{a} & \text{for a circular waveguide} \end{cases}$$

Similarly to the position of the conductor the impedance of the waveguide and coaxial feed may not always be properly matched. To alter the impedance of the transition the dielectric may be positioned further down in to the waveguide to alter the impedance transition, as well as change the insertion of the conductor. There is more information about this in [11] for the interested reader.

3

Design and manufacturing of the feed

In this thesis project a dual band single polarization antenna feed for parabolic reflectors is designed and manufactured. The design process is focused on the transition and excitation of the lower frequency band. Excitation of E-band is achieved by a rectangular to circular waveguide transition obtained from LEAX Arkivator Telecom AB, and is thus not included in this design process. A large focus during the design process was to keep it simple and cheap to manufacture, and thus the most optimal solution for good performance is not always preferred, as this may increase the cost of the feed.

The design was conducted in a chronological order, i.e. the circular transition between the upper and lower band waveguides was designed, and was used as the base structure throughout the project. Thereafter different solutions for excitation of the lower band was investigated.

3.1 Design of E-band feed and waveguide

The upper band covers the frequencies of 71-76 GHz and 81-86 GHz. The E-band feed is a waveguide feed as it was discussed that a coaxial feed could be too expensive and time-consuming to investigate thoroughly. Coaxial feeds also have a tendency to have higher losses, and are very sensitive to manufacturing errors. Thus it was settled for a waveguide feed. The upper band is excited by a rectangular waveguide feed which has been previously used by LEAX Arkivator Telecom, and is the standardized UBR740.

3.1.1 E-band waveguide transition

The E-band waveguide transition is the transition between the upper and lower band waveguides. The main complication in this design step is the higher order modes which can propagate in the larger waveguide, as well as the simulation time for the E-band. The initial dimensions for the circular waveguides were provided by LEAX Arkivator Telecom. These are 1.5875mm for the inner radius of the E-band waveguide, and 6.947mm inner radius for the 18GHz-band waveguide. Thus the 18 GHz waveguide is approximately 4.5 times larger than the E-band waveguide, and can sustain more than 20 modes according to CST Microwave Studio at E-band.

Since the 18 GHz waveguide is highly overmoded for the E-band, the transition should be designed such that it does not excite the higher order modes. Generally to avoid higher order mode generation the transition between the waveguides should be smooth, symmetrical and long, as this does not disturb the field within the waveguide, and any deviation or asymmetry in the design may induce higher order modes and thus affect the performance of the feed. However, it is not feasible to manufacture a transition that is too long, and thus it is a matter of manufacturability that limits the length in this design, which was set to be 60mm.

To achieve an efficient optimization routine which minimizes the generation of higher order modes a curvature with a high degree of freedom had to be used, with a low amount of optimization parameters. For this design a Bézier curve was used. [7] A Bézier curve is a one- or two-dimensional parametric curve defined by n polynomials, defined accordingly:

$$\mathbf{B}(t) = \sum_{i=0}^n \binom{n}{i} (1-t)^{n-i} t^i \mathbf{P}_i \quad (3.1)$$

For this design a Bézier curve of the third order was used, i.e.:

$$\mathbf{B}(t) = (1-t)^3 \mathbf{P}_0 + 3(1-t)^2 t \mathbf{P}_1 + 3(1-t) t^2 \mathbf{P}_2 + t^3 \mathbf{P}_3$$

Where the points \mathbf{P}_0 , \mathbf{P}_1 , \mathbf{P}_2 and \mathbf{P}_3 define points in the space between the E-band waveguide and 18GHz waveguide. In the figure below the curvature of two Bézier defined curves can be seen based on the points \mathbf{P}_0 to \mathbf{P}_3 .

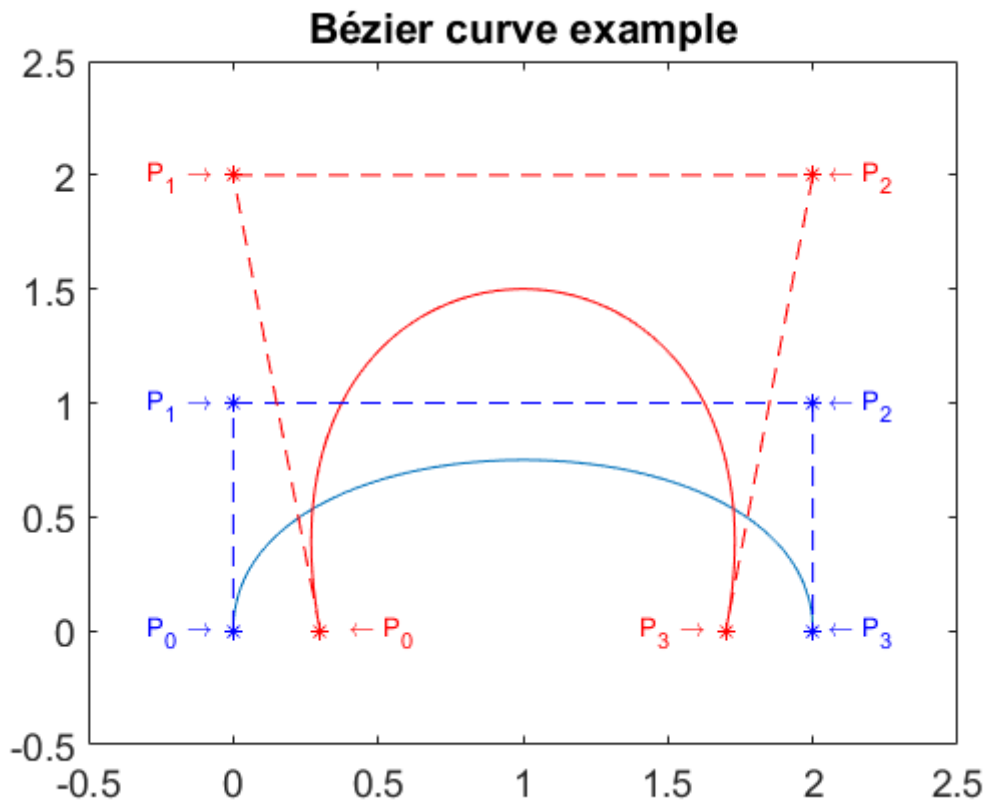


Figure 3.1: Two cubic Bézier curves with different defining points. The dashed lines represent the lines between each point, and the lines the resulting Bézier curves.

However, as can be seen from the figure \mathbf{P}_0 and \mathbf{P}_3 are defining the starting and end points of the Bézier curve, i.e in this case, \mathbf{P}_0 should be at the inner E-band waveguide radius and the beginning of the transition. \mathbf{P}_3 should be at the inner 18 GHz waveguide radius and the end of the transition. This gives thus four different parameters to optimize the curvature of the waveguide and was deemed enough, as increasing the number of parameters available for optimization might increase the optimization time.

Additionally to reduce the optimization time of the curvature the optimization goal was focused on increasing the transmission and decreasing the reflection coefficient, rather than decreasing all the higher order modes and reflection coefficient. This was to reduce the amount of optimization goals to two instead of having more than 20 goals. The finalized optimization can be seen in the figure below, along with the yielded results:

3. Design and manufacturing of the feed

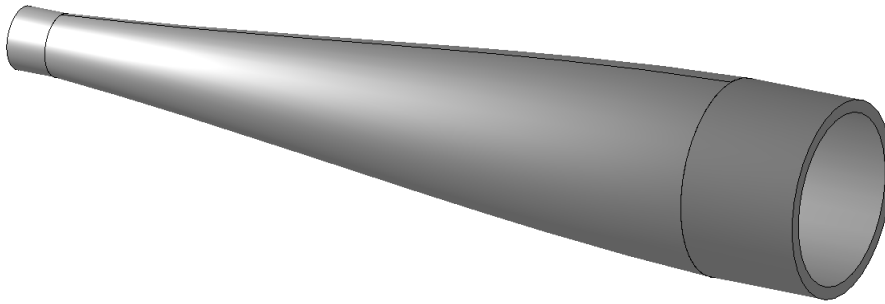


Figure 3.2: Visualization of the optimized E-band transition with a Bézier profile.

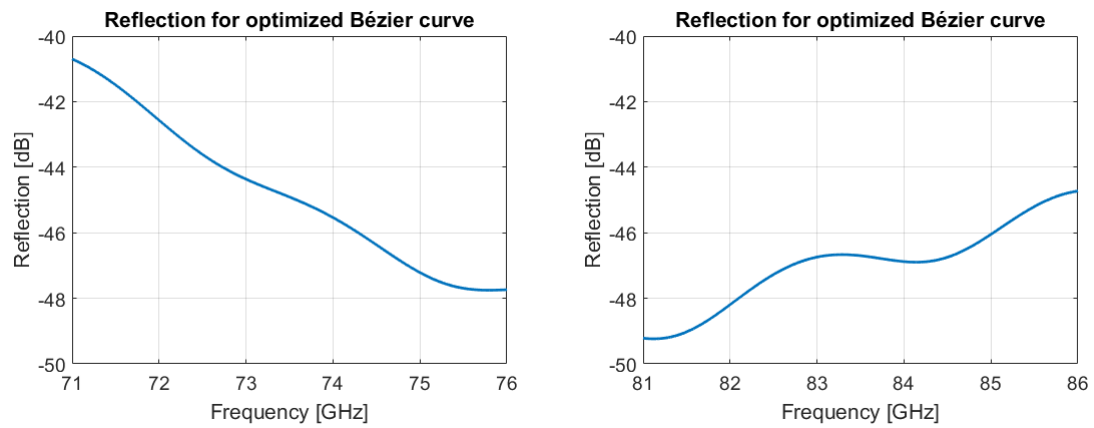


Figure 3.3: The reflection coefficient for the feed after optimization.

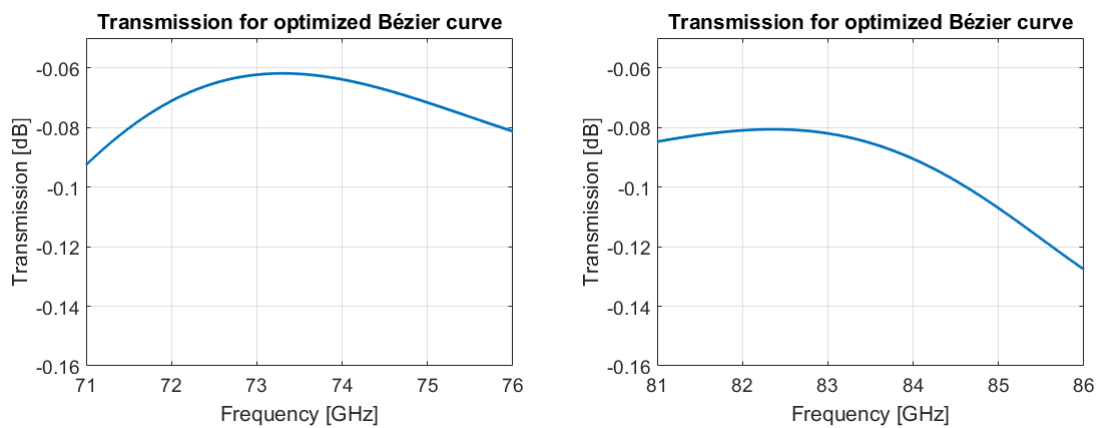


Figure 3.4: The transmission coefficient for the feed after optimization.

3.2 Design of 18 GHz-band excitation

The lower band covers the frequencies between 17.7-19.7 GHz. In this section two different concepts will be presented as they were both thoroughly investigated. Different problems will be discussed and the final solution presented. The E-band transition is used as the basic design for both of these concepts. As was previously mentioned in the demarcation an OMT was not investigated, but can for the interested reader be read more about here [8], here [9] and here [10].

3.2.1 Coaxial feed with ridges

A benefit of using a ridged waveguide for the excitation is that the coaxial feed can be placed inside the ridges. There are many solutions already presented in this field which simplifies the design, see e.g.: [12], [13] and [14]. However, all of these solutions use an electrical wall for the reflection of the power. This is not suitable when combining coaxial feed with a waveguide feed.

The idea behind this design is to use the cut-off properties of the waveguide as an electric wall to reflect the power instead of having an electric wall for the 18 GHz band. If the design is successful for one polarization it should be re-designable for the other polarization with some changes and thus function as a dual-polarized setup without too much effort. However, the problem with this design is that the introduction of ridges introduces discrepancies in the structure which may excite higher order modes. The design process and results are presented below.

3.2.1.1 Ridge design

It is beneficial if the design curve of the ridges are, similar to that of the waveguide curve, simple but with a high degree of freedom. Investigation of previous publications showed that the following equation was suitable for this design [13]:

$$x = O + \frac{H}{2(e^{RL} - 1)}(e^{Rz} - 1) \quad (3.2)$$

Where the length of the ridge is given by L and the diameter of the waveguide is given by H . R is the opening rate of the ridge, and is thus implying how fast the ridge is opening, see figure 3.5.

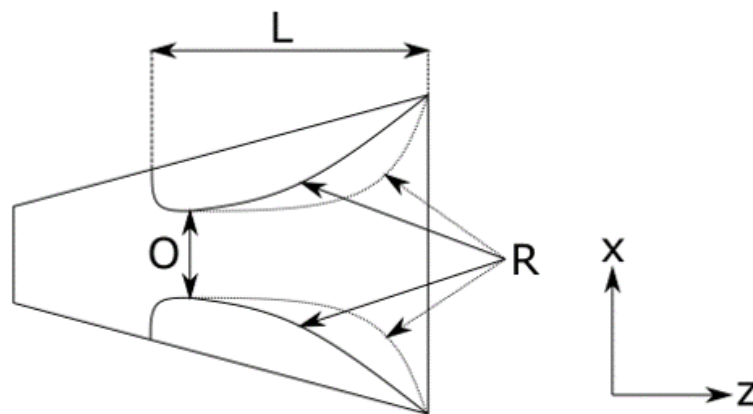


Figure 3.5: An explanation of the mathematical curve used for the ridge design. O is the ridge opening, R shows two different opening rates, where the dotted one has a higher opening rate, and L shows the length of the ridges.

Thus the curvature of the ridge can be optimized and designed for. The width of the ridges are limited on the lower end by the coaxial conductor width, and larger end by the waveguide dimensions. The length is limited by the length of the waveguide. Since the E-band transition is sensitive to small changes within the structure the ridge should be as smooth as possible. The optimized ridge curvature can be seen in figure 3.6.

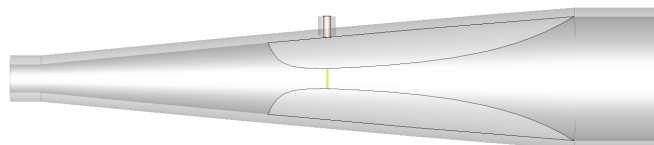


Figure 3.6: The optimized structure with ridges and coaxial feed.

Where the feed opening at the coaxial feed is 1.5mm, the total length of both ridges are approximately 28mm, and the opening rate is 0.1. The length of the reversed ridge is 6.5mm and the opening rate is 0.85. The width of both ridges are 1 mm thick, and are limited by the coaxial dielectric in thickness. The dimensions of the coaxial feeds conductor and dielectric were chosen to be thin, and commercially available. The most suitable feed found had an inner conductor diameter of 0.29mm, and dielectric diameter of 0.92mm.

The back-section of the ridge curvature was designed to be approximately a quarter-wavelength long in order to use the cut-off properties of the waveguide as an electric wall. The resulting performance of the coaxial ridge-feed can be seen in figure 3.7.

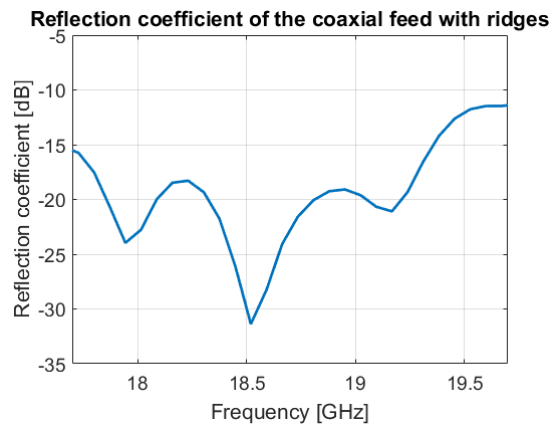


Figure 3.7: The resulting reflection coefficient of the coaxial feed in the optimized structure with ridges.

Where the total reflection coefficient is better than -11.5 dB.

3.2.1.2 E-band performance

As was mentioned previously the E-band performance is affected by the introduction of ridges. The result of the E-band simulation can be seen in figure 3.8, and 3.9.

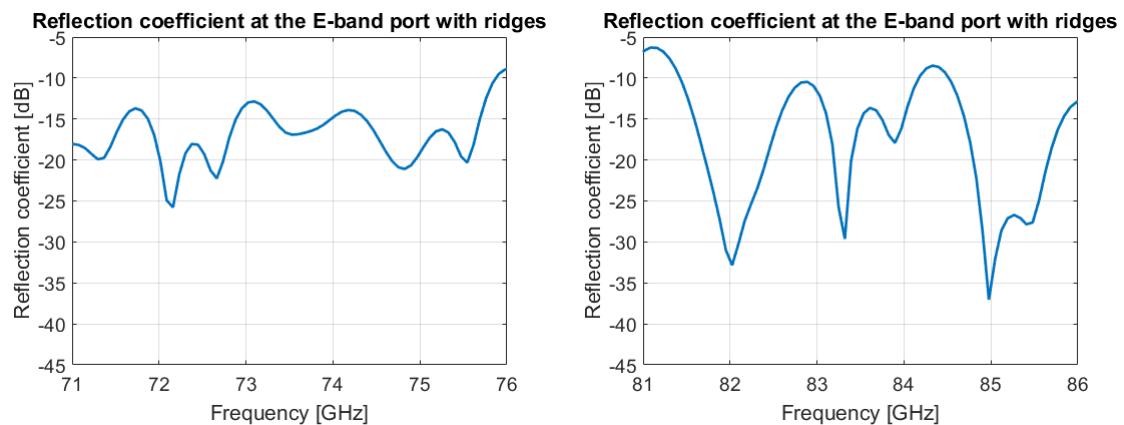


Figure 3.8: The resulting reflection coefficient seen from the E-band port in the optimized structure with ridges.

3. Design and manufacturing of the feed

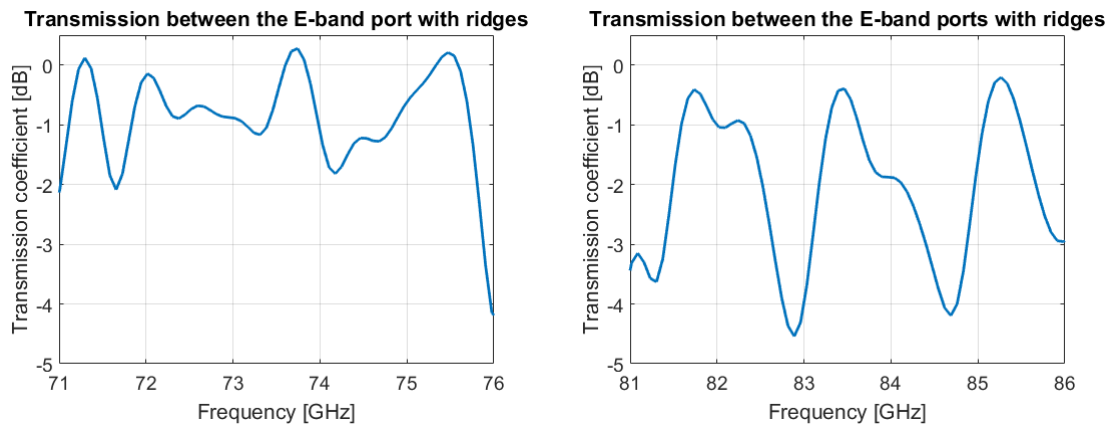


Figure 3.9: The resulting transmission coefficient between the E-band ports in the optimized structure with ridges.

As can be seen, the reflection coefficient is better than -6 dB for the entire band, and the transmission coefficient is better than -4.5 dB for the entire band. These results were deemed to not be good enough, as more than half the power is lost for certain frequencies. When these results were obtained the design for the lower band feed was changed.

However, simulations were also made where the 18 GHz-band was ignored, and the ridge design was highly optimized for E-band, see figure 3.10, 3.11. Here it can be seen that the system may be usable for E-band.

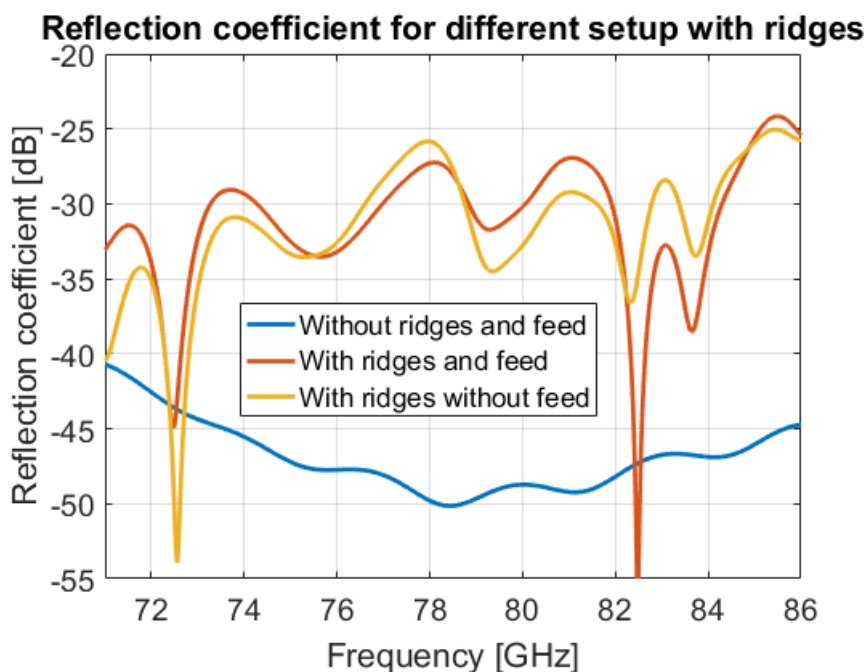


Figure 3.10: The resulting reflection coefficient between at the E-band port with ridges optimized for E-band.

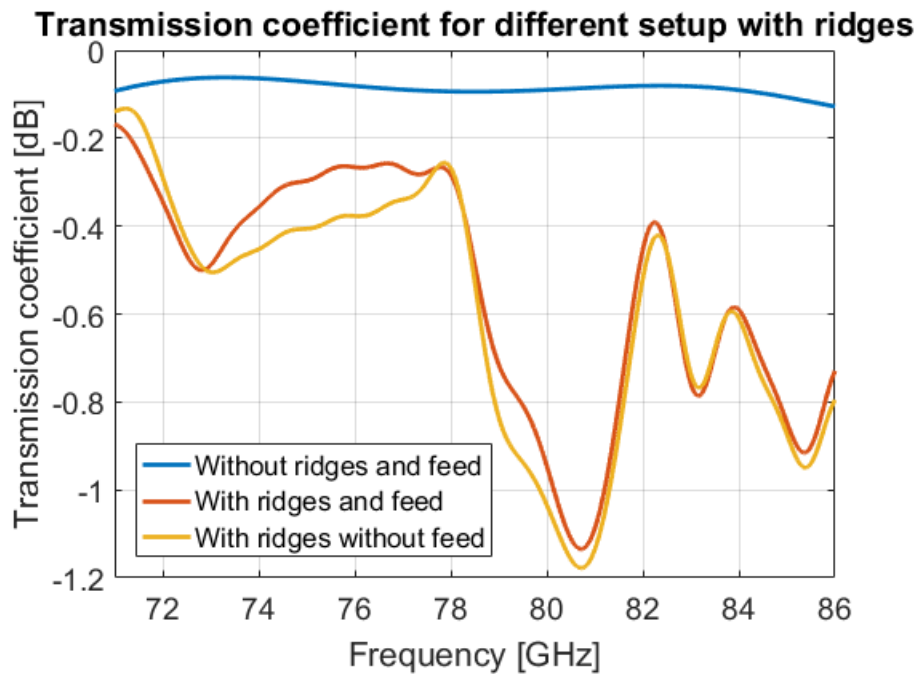


Figure 3.11: The resulting transmission coefficient between the E-band ports with ridges optimized for E-band.

Which shows that this design setup can be used at E-band. However, for this design the coaxial feed did not achieve suitable results. For these results (figure 3.10, figure 3.11) the ridges were extended in length, the feed opening was larger, and the width and opening rate smaller, compared to figure 3.8.

3.2.2 Coaxial feed without ridges

As the performance of the ridge design did not achieve sufficiently good results, another design was tested for the coaxial feed. As was mentioned earlier in section 2.3.2 an ordinary coaxial feed uses a backshort, which is, ideally, a perfect electric wall, to reflect the power transmitted by the coaxial feed to create a standing wave pattern in order to improve the performance. For this second design a pin-structure is introduced within the transition in order to work as a single-polarized electric wall for the 18 GHz-band. A schematic figure can be seen in figure 3.12

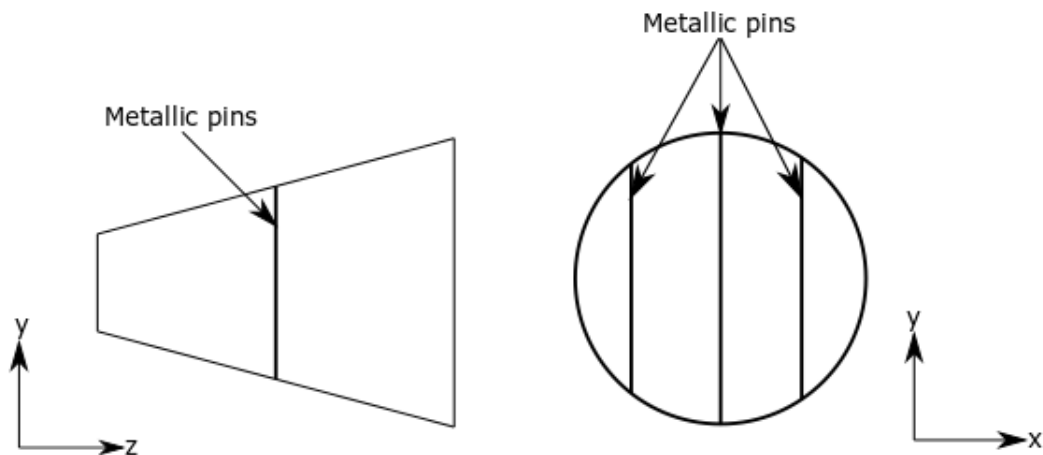


Figure 3.12: A schematic figure showing the setup of the pin structure concept, which acts as a single-polarized electrical wall.

The benefit of using this is that if the metallic pins are thin enough and positioned correctly, the orthogonally polarized E-band should not be affected noticeably by them. However, the drawback is that this design does not support a dual band solution, since the metallic pins would then be parallel with the electric field of the E-band and reflect a portion of the power and reduce the performance of the E-band.

The transition was kept, similarly to the ridges, as initially designed. The main design steps of the pin structure was to find the position of the metallic pins and coaxial feed, the number of pins used, the relative distance between the pins and feed, the thickness of the pins, and the insertion of the coaxial conductor and dielectric in the waveguide. These steps are explained more in detail below.

3.2.2.1 Pin structure design

The approximate positioning of the coaxial feed and pin structure was found by investigating the cut-off frequencies along the transition. The pin-structure and coaxial feed was spaced approximately a quarter-wavelength apart. The pins dimensions, distance between and relative distance to the coaxial feed, as well as the insert length of the coaxial conductor and dielectric was thereafter simulated and optimized for. Clarification of the parameters that were optimized for can be seen in figure 3.13.

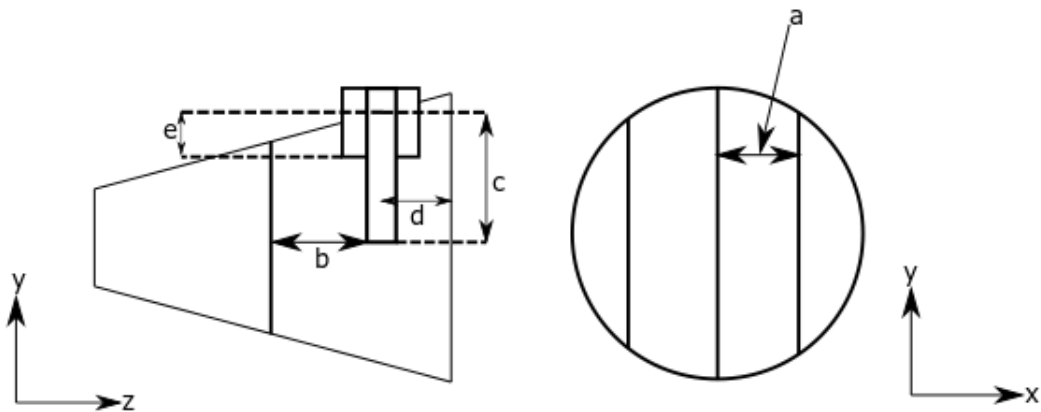


Figure 3.13: A schematic figure showing the parameters that were optimized for in order to improve results. "a" is the pin displacement, "b" is the relative distance between the pin wall and coaxial feed. "c" is the insert length of the coaxial conductor, "d" is the offset from the end of the transition, and e is the insert length of the coaxial dielectric. The thickness of the pins is the width in x-direction, and length is the width in y-direction.

Initially the pin displacement was tested at 18 GHz. The result can be seen in figure 3.14.

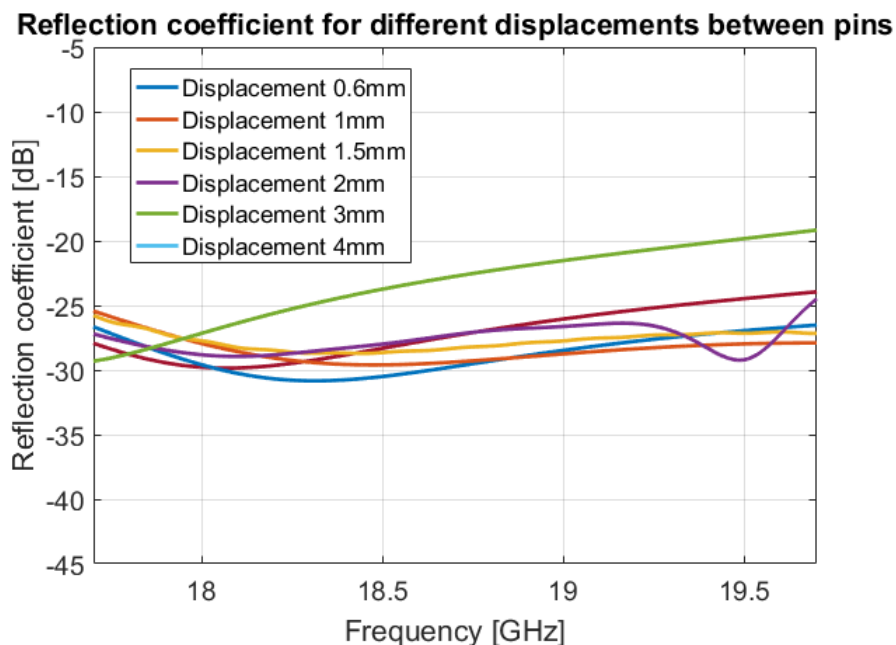


Figure 3.14: The reflection coefficient for different pin displacement around 18 GHz.

Which shows that the pin displacement does not affect the performance significantly

3. Design and manufacturing of the feed

at 18 GHz when the thickness is constant.

The thickness was briefly tested as well. The result can be seen in figure 3.15.

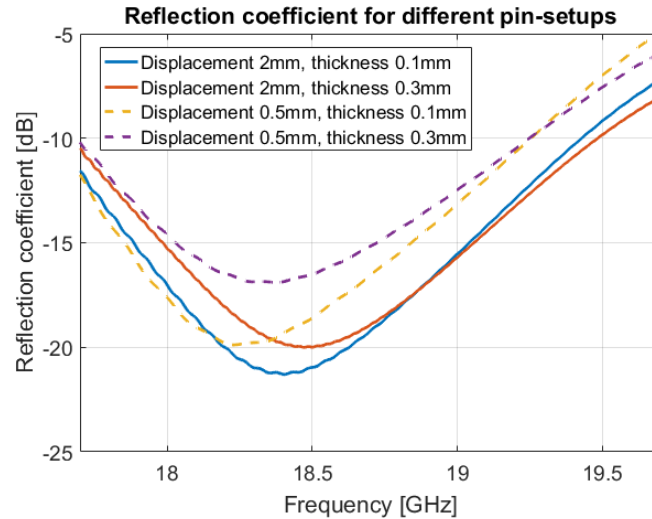


Figure 3.15: The reflection coefficient for different pin setups.

Which shows that the result is dependant on thickness and relative displacement. Thus it is important to not have a small displacement with a large width, as this affects the results negatively. The performance impact of the other parameters is not shown in the same detail as for the pin displacement and thickness, as these are more commonly optimized in coaxial feed solutions. Instead the other parameters were optimized for. For the pin-setup three different geometries were investigated as well for manufacturing purposes. This is due to the different manufacturing methods that may prefer certain geometries over others. The result for three different geometries can be seen in figure 3.16

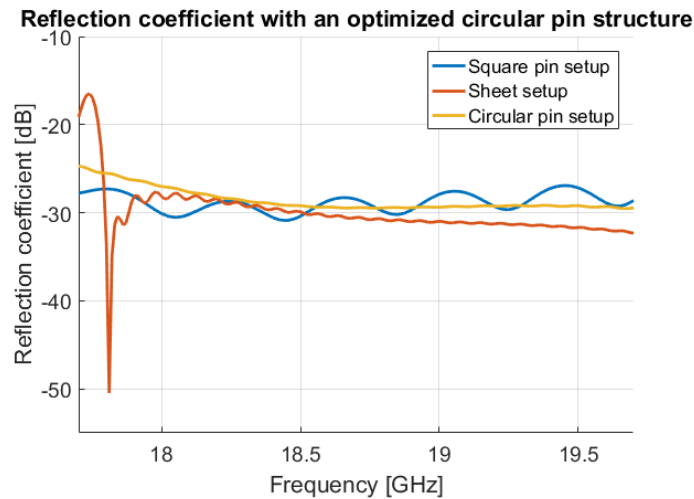


Figure 3.16: The reflection coefficient for different pin geometry setups. For all cases the coaxial conductor insert is 3.3mm, the dielectric insert is 0mm, the distance between the pin wall and conductor is 5.9mm and the thickness is 0.2mm. For the sheet-case the length of the pins are 1mm.

The parameters are similar for all three cases, and as can be seen in this case all three geometries have similar results, and the circular and square case are better than -25dB for the entire band. The sheet case has a degraded performance relative to the others, but can be optimizeable for the band.

3.2.2.2 E-band performance

The E-band performance for the different geometries can be seen in figure 3.17.

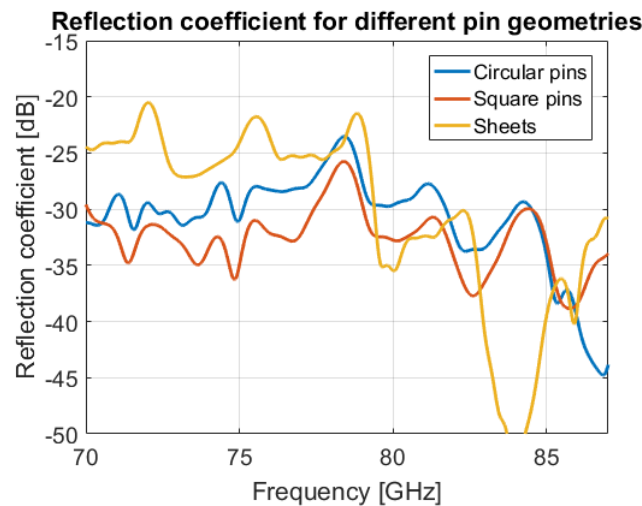


Figure 3.17: The reflection coefficient for different pin geometries at E-band.

As can be seen the performance of the sheet structure is worse. Circular and square-pin structure have similar performance and is better than -27 dB in-band.

The impact of the thickness was also investigated for E-band. The result can be seen in figure 3.18.

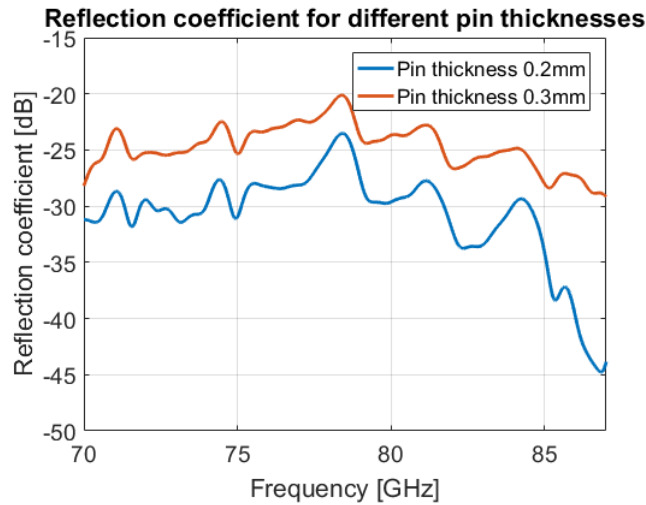


Figure 3.18: The reflection coefficient for different pin thicknesses at E-band

Which shows a result that is approximately 5 dB worse for a 0.1mm increase in thickness of the pins. Thus the performance is highly dependant on the thickness of the pins, which is not surprising since an increase in thickness will make the structure more prominent for the orthogonal polarization.

3.3 Manufacturing

This section will discuss and present the manufacturing of the antenna feed. The manufacturing was discussed and planned together with mechanical engineers at LEAX Arkivator Telecom AB in order to have a manufacturable feed with sufficient tolerances. The finalized structural layout is changed slightly from the previously simulated structure. All results for the manufacturable design will be presented in chapter 4.

3.3.1 E-band transition

The E-band transition was designed with manufacturability in mind, i.e. the length was limited, as well as the outer and inner dimensions of the waveguide are matched to standardized dimensions for LEAX for simplicity in the manufacturing process. For the manufacturing the structure will be drilled, which requires a drill that is at least as long as the waveguide, and as thin as the innermost diameter.

3.3.2 18 GHz excitation

The coaxial feed used in the design process was an off-the-shelf product from rosenberger. Details of the feed can be seen in Appendix A. The coaxial conductor insert is longer than the base length of the stripped conductor from the manufacturer.

Re-simulating shows that the performance with a part of the dielectric insert in the structure in order to keep the conductor length similar shows that the result is tolerable. It is also possible to cut the conductor or dielectric to the desired length. However, the tolerances may not be as high as needed. The most suitable solution would be to have a customized order of the coaxial feed, but that will increase the cost and is not necessary for a concept design.

3.3.2.1 Pin structure

In order to realize the pin structure the design had to be changed slightly. In the simulated case the pins were inserted in the structure as three separate objects. However, drilling holes that are 0.2mm thin with a high tolerance is not feasible. The design was changed such that the E-band transition is split in two parts, and the split is positioned at the simulated pin structure position. The pins themselves were re-designed to be a separate structure which is etched from a circular thin metal plate. This process can then offer a tolerance which is high enough while simultaneously keeping the thickness of the metal plate thin. A schematic exaggerated explanation of the new transition can be seen in figure 3.19.

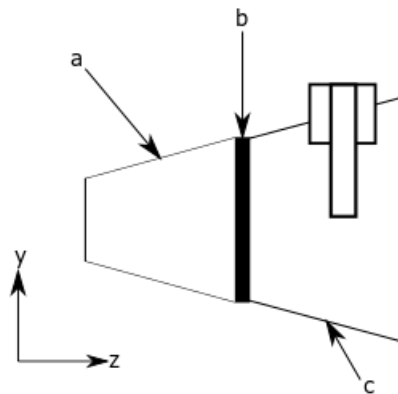


Figure 3.19: A schematic figure showing the new design. The sections "a", "b", and "c" are manufactured in three separate processes. The E-band port is the leftmost part, i.e. start of "a".

This design extends the length of the structure by approximately 0.2mm, as the pin structure is flat and positioned between the waveguide transitions.

3.3.3 Finalized structure

The finalized mechanical structure is thus designed. It is separated in four different parts, whereas three of them have been simulated and designed in this project. The fourth part is a transition from a rectangular to circular waveguide provided by LEAX. The final mechanical design of the antenna feed can be visualized in figure 3.20, and 3.21.

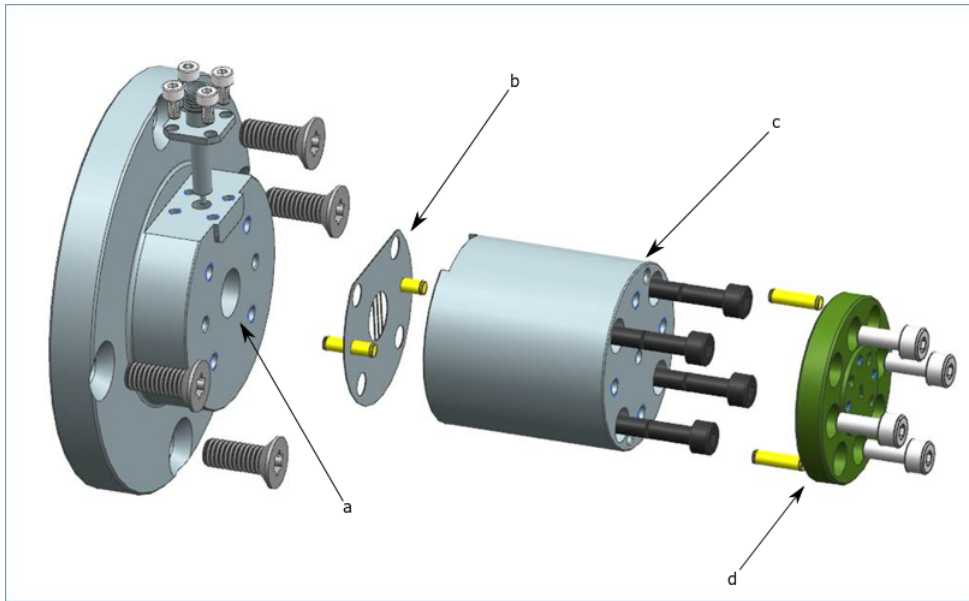


Figure 3.20: The mechanical design of the antenna feed. The sections "a", "b", and "c" are manufactured in three separate processes. Section "d" is the rectangular to circular transition obtained by LEAX Arkivator Telecom AB.

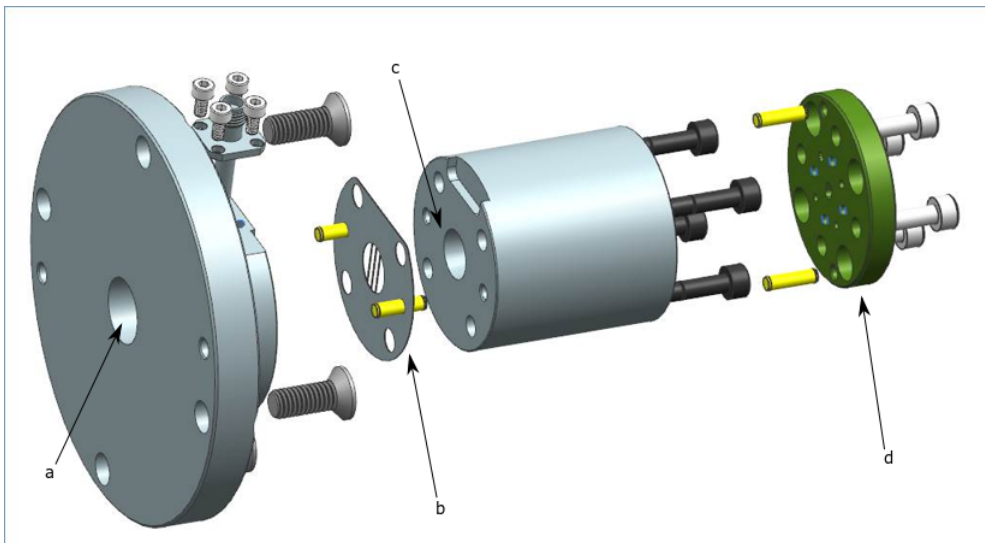


Figure 3.21: The mechanical design of the antenna feed. The sections "a", "b", and "c" are manufactured in three separate processes. Section "d" is the rectangular to circular transition obtained by LEAX Arkivator Telecom AB.

4

Results

This section will present the results of the finalized structure, i.e. the feed which was split in three sections, which was described in chapter 3, as well as the measured results from the manufactured antenna feed. The results will be presented with and without the sub reflector. For the results with it should be kept in mind that the sub reflector is not optimized for the antenna feed.

A 3D-model of the simulated structure with and without hat feed can be seen in figures 4.1, and 4.2. The structure seen in this figure is not circular and smooth. This is to simplify the parametrization in CST, the manufactured structure will not have these distinct circular sections, but rather be as smooth as possible.

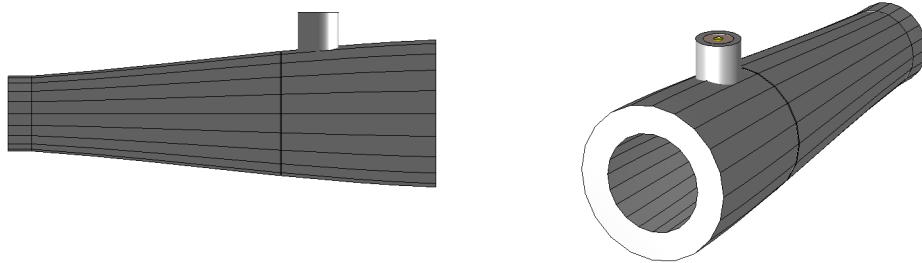


Figure 4.1: The finalized structure simulated in CST without the sub reflector.

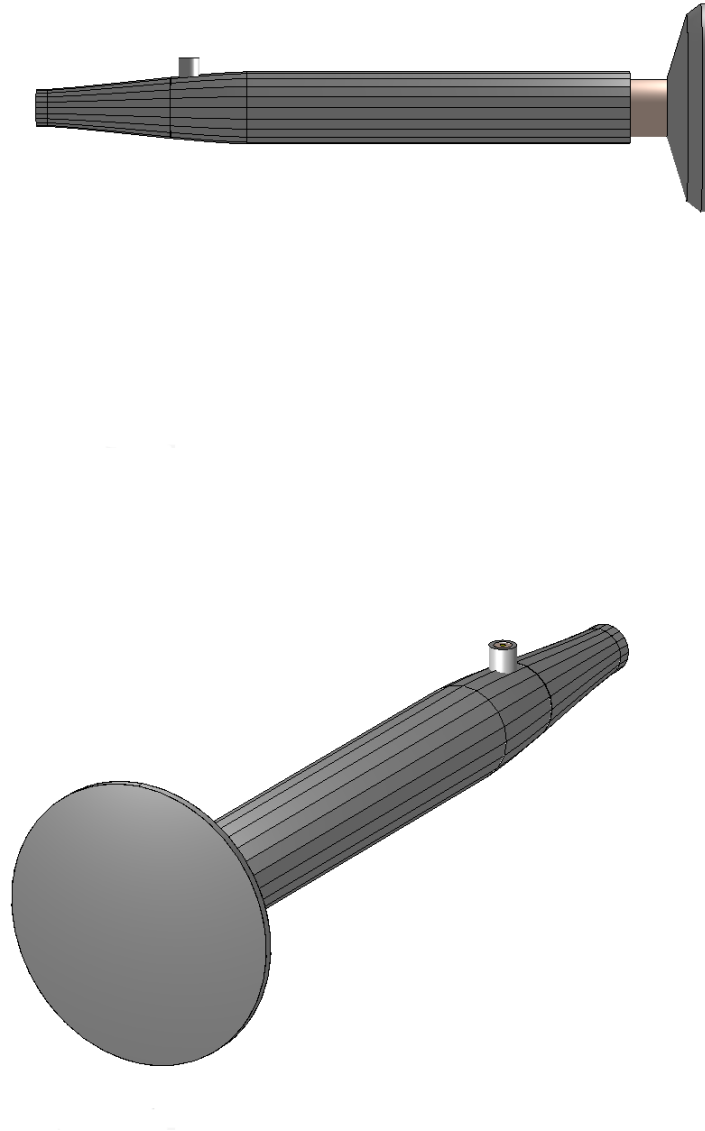


Figure 4.2: The finalized structure simulated in CST with the sub reflector.

4.1 18 GHz band

This section presents the reflection coefficients, 3-dimensional far field, and E- and H-plane cuts with and without the sub reflector, as well as the efficiencies with the sub reflector.

The simulated reflection coefficient for the 18 GHz-band port to port simulation

can be seen in figure 4.3

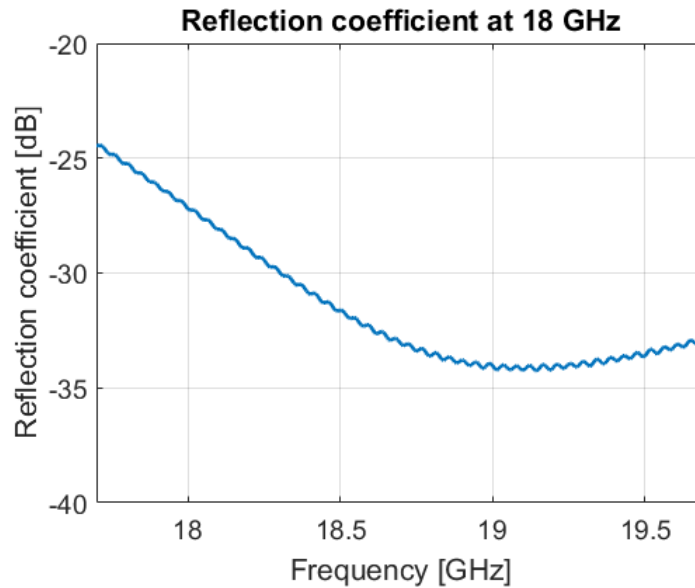


Figure 4.3: The simulated reflection coefficient for the 18 GHz-band port to port simulation

The simulated reflection coefficients when analyzing the feed as a horn antenna can be seen in figure 4.4.

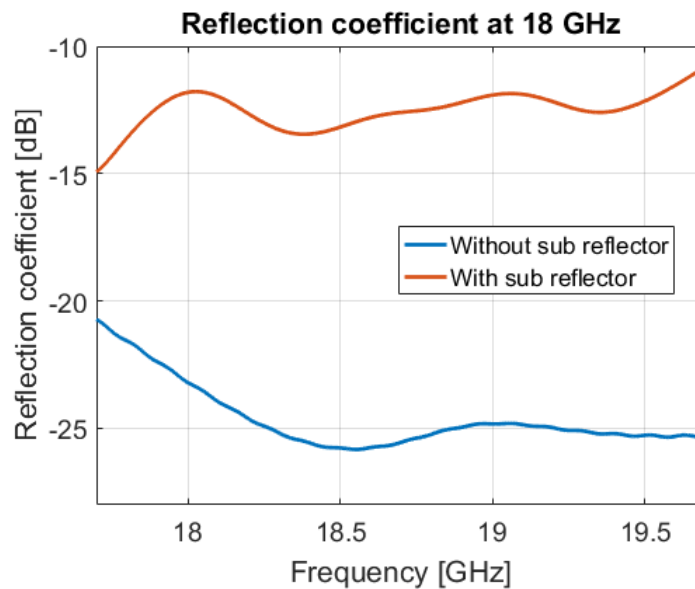


Figure 4.4: The simulated reflection coefficients for the 18 GHz-band horn antenna simulation with and without sub reflector.

The result when including the sub-reflector is worse. As mentioned previously the sub reflector is not optimized for this antenna feed, and thus will have a large negative impact on the result.

In table 4.1 the efficiencies can be found for the lower band.

freq (GHz)	e_{sp}	e_{ill}	e_{pol}	e_{ϕ}	e_{ap}
17.7	97 %	89%	93%	82%	66%
18.7	98%	89%	91%	82%	65%
19.7	99%	89%	92%	84%	68%

Table 4.1: The efficiencies for the simulated antenna feed with sub reflector.

4.1.1 Far field results

In the figures below the cartesian farfield plots and 3D-farfield plots can be seen for three different frequencies for the simulated structure without the sub reflector.

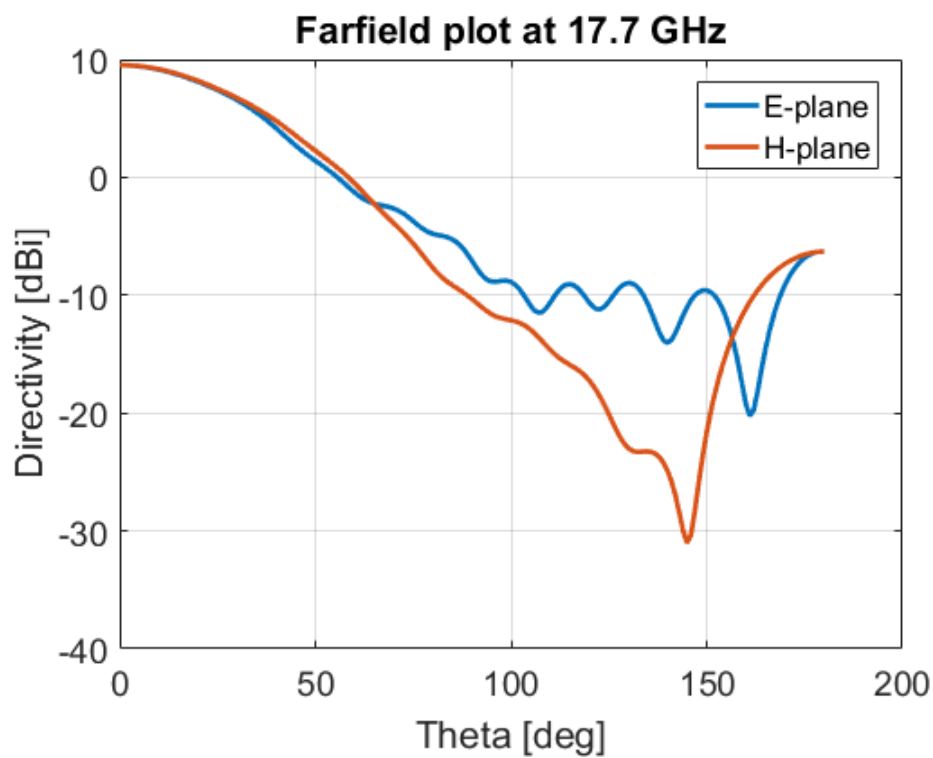


Figure 4.5: Farfield plot of the antenna feed at 17.7 GHz

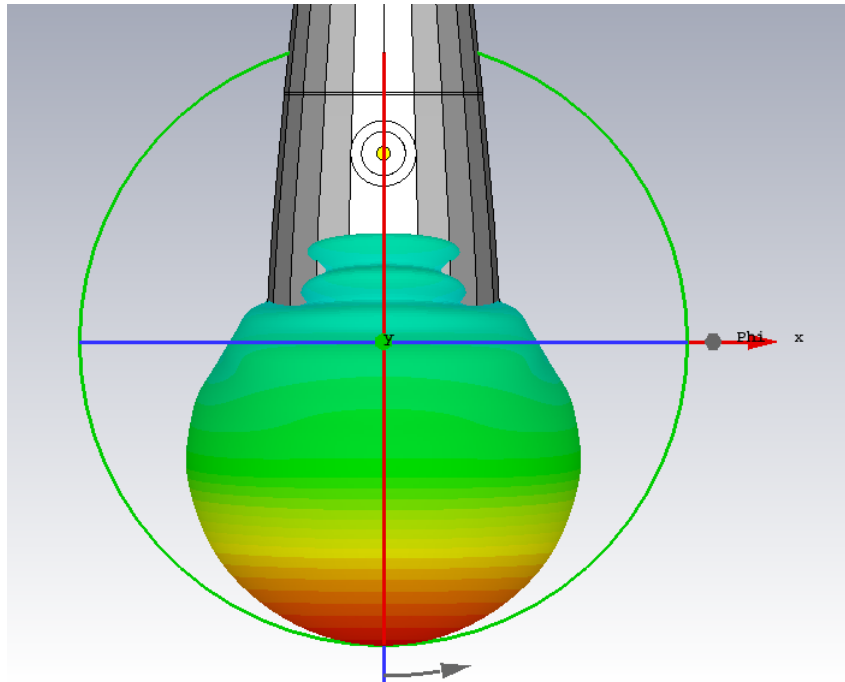


Figure 4.6: 3D Farfield plot of the H-plane of the antenna feed at 17.7 GHz

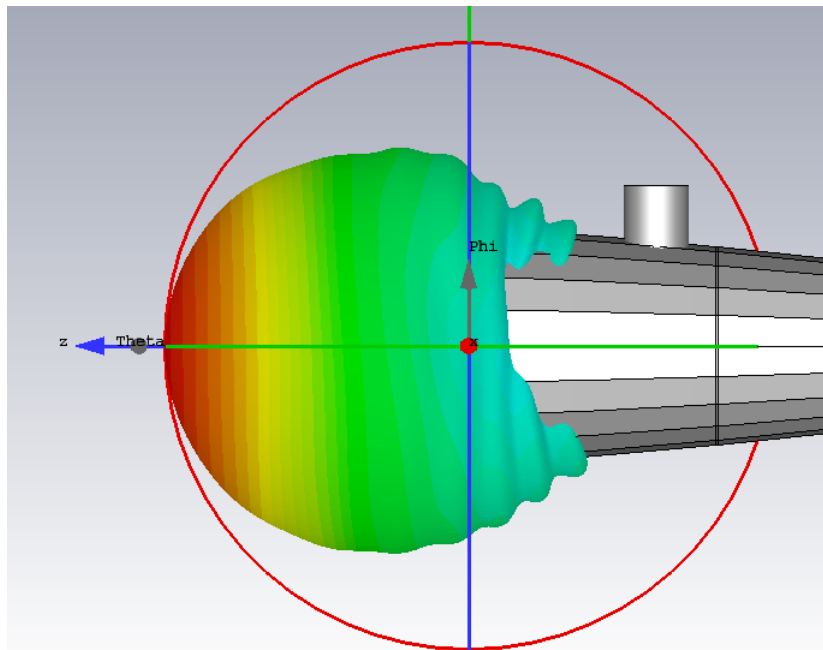


Figure 4.7: 3D Farfield plot of the E-plane of the antenna feed at 17.7 GHz

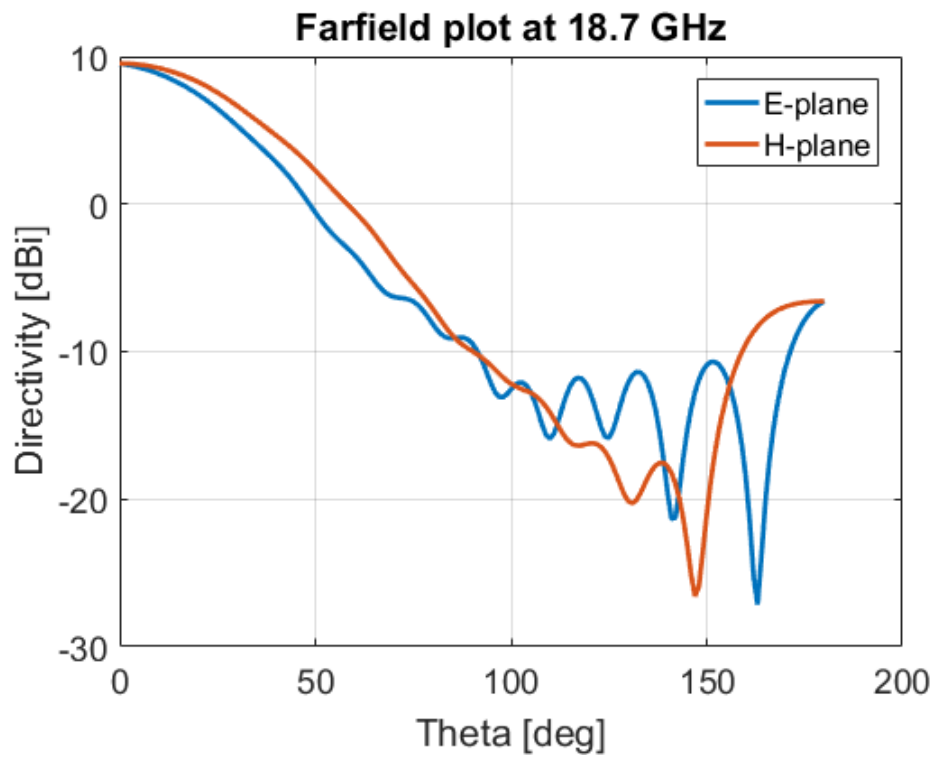


Figure 4.8: Farfield plot of the antenna feed at 18.7 GHz

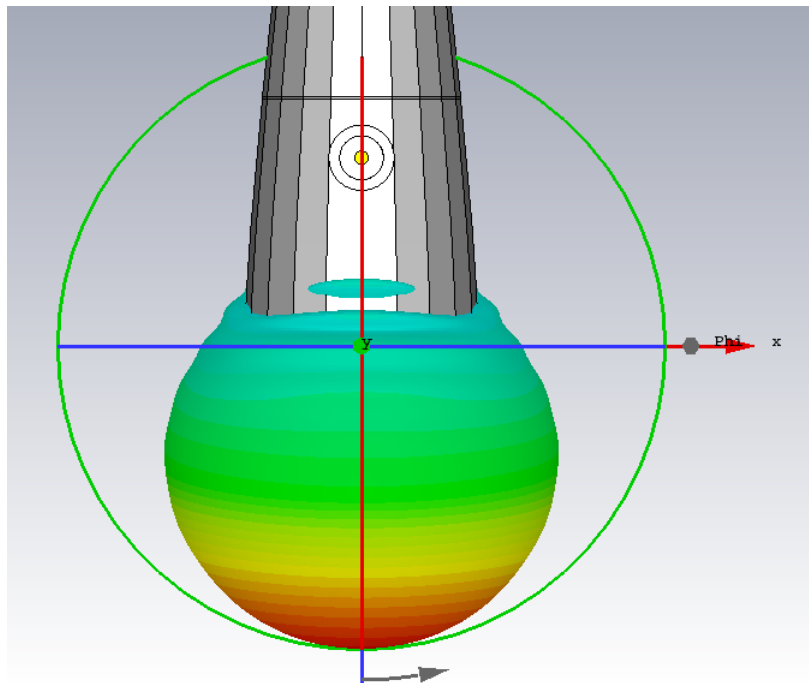


Figure 4.9: 3D Farfield plot of the H-plane of the antenna feed at 18.7 GHz

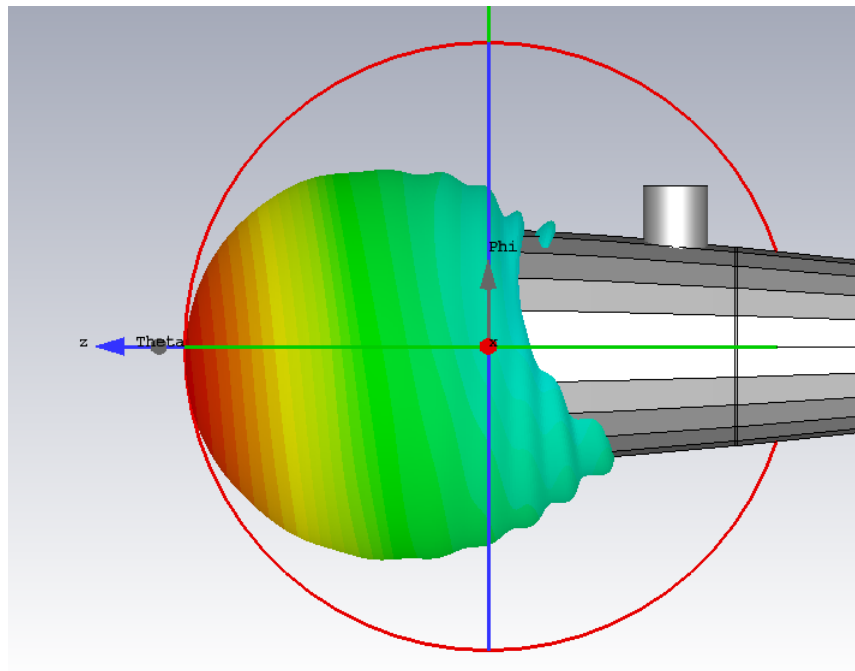


Figure 4.10: 3D Farfield plot of the E-plane of the antenna feed at 18.7 GHz

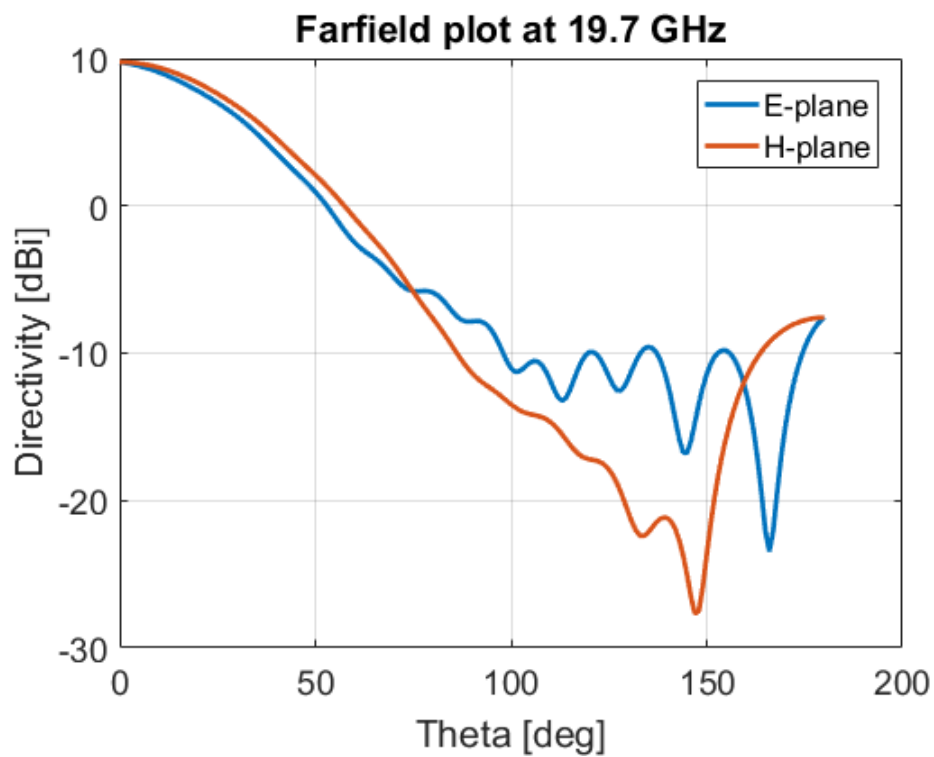


Figure 4.11: Farfield plot of the antenna feed at 19.7 GHz

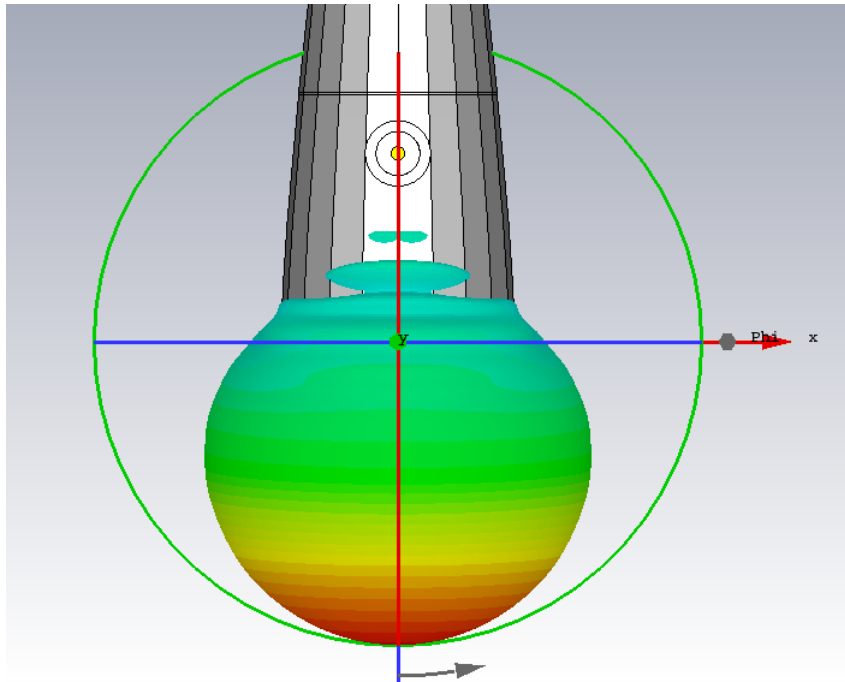


Figure 4.12: 3D Farfield plot of the H-plane of the antenna feed at 19.7 GHz

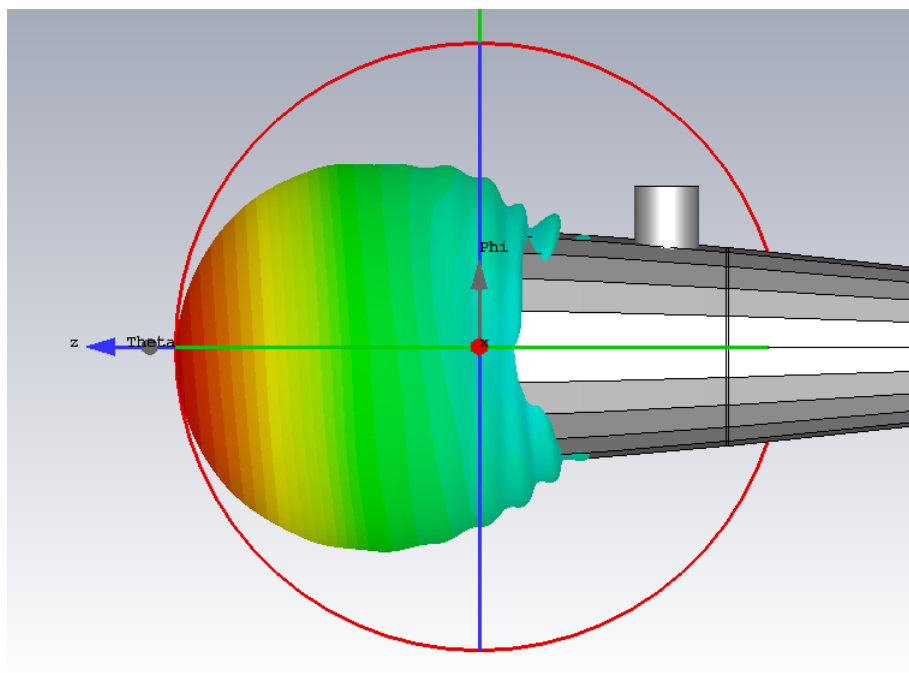


Figure 4.13: 3D Farfield plot of the E-plane of the antenna feed at 19.7 GHz

In the figures below the same simulations can be seen at 18 GHz with the sub reflector.

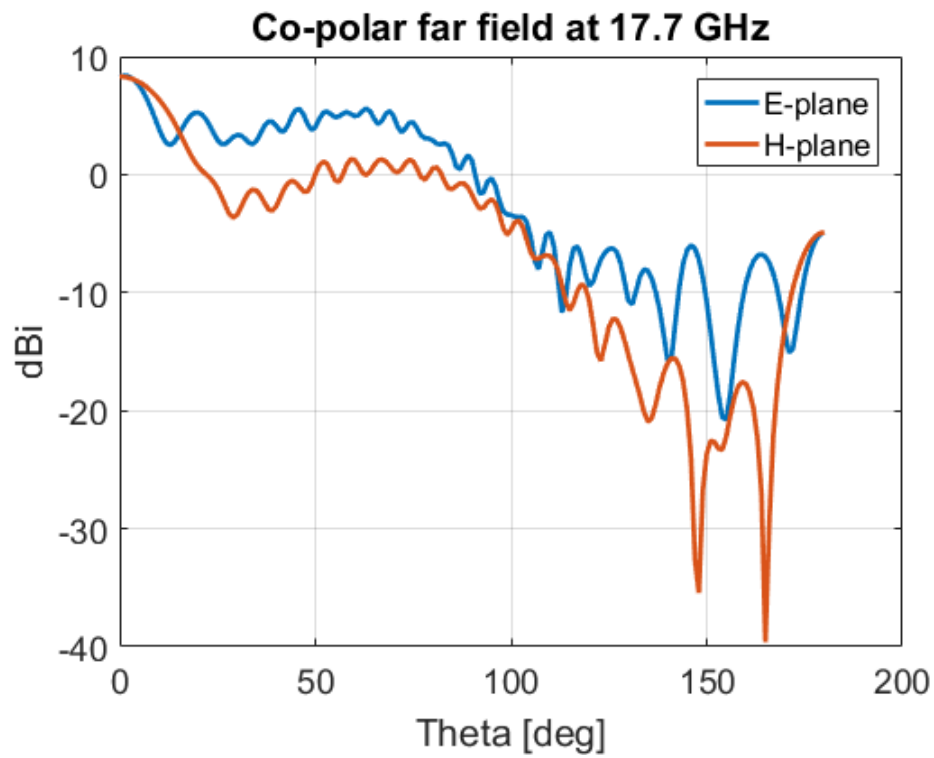


Figure 4.14: Farfield plot of the antenna feed with the sub reflector at 17.7 GHz. The angle is reversed, and 180 degrees is forward.

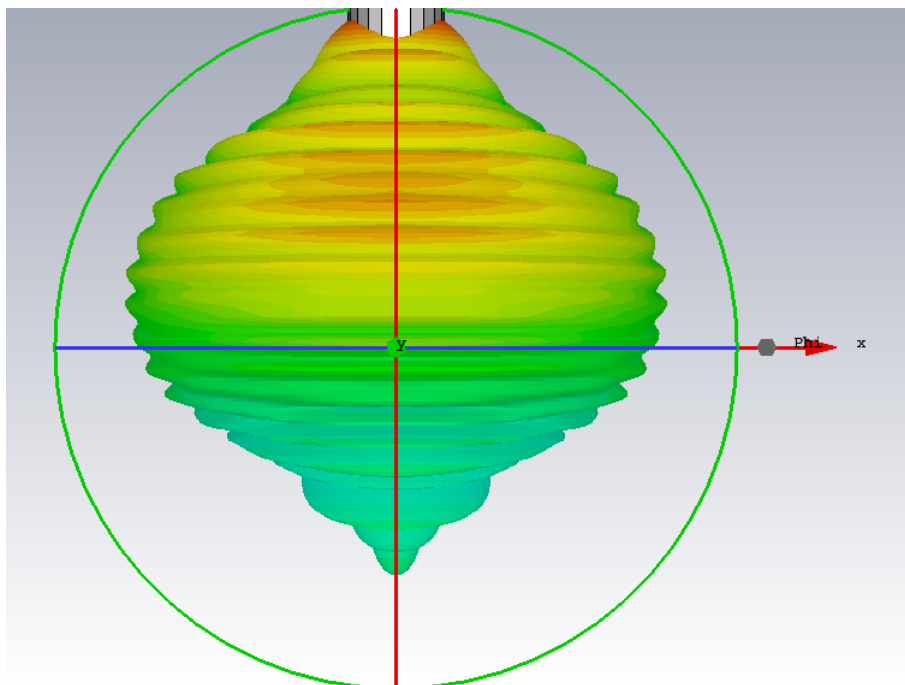


Figure 4.15: 3D Farfield plot of the H-plane of the antenna feed with the sub reflector at 17.7 GHz

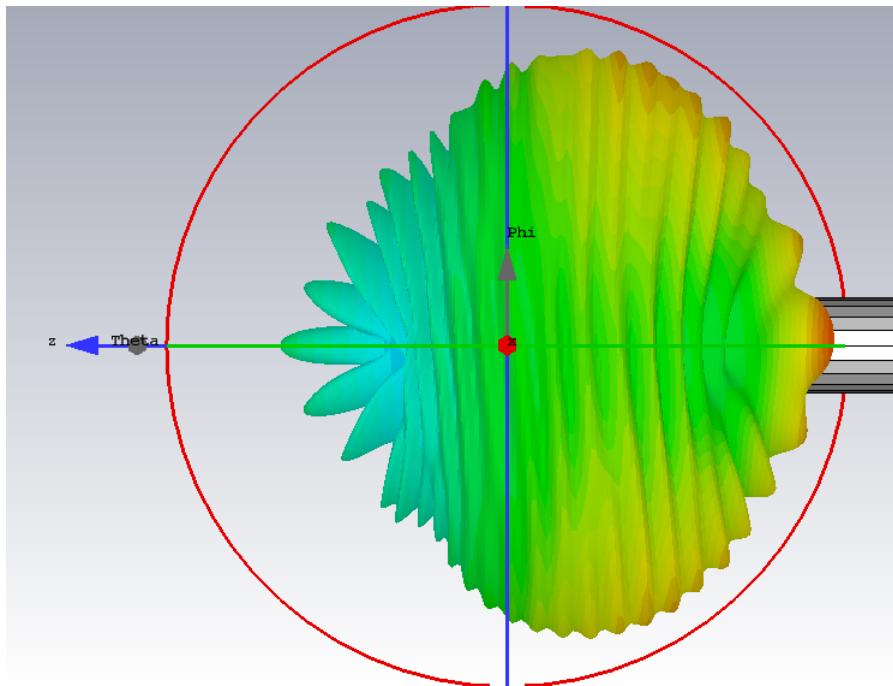


Figure 4.16: 3D Farfield plot of the E-plane of the antenna feed with the sub reflector at 17.7 GHz

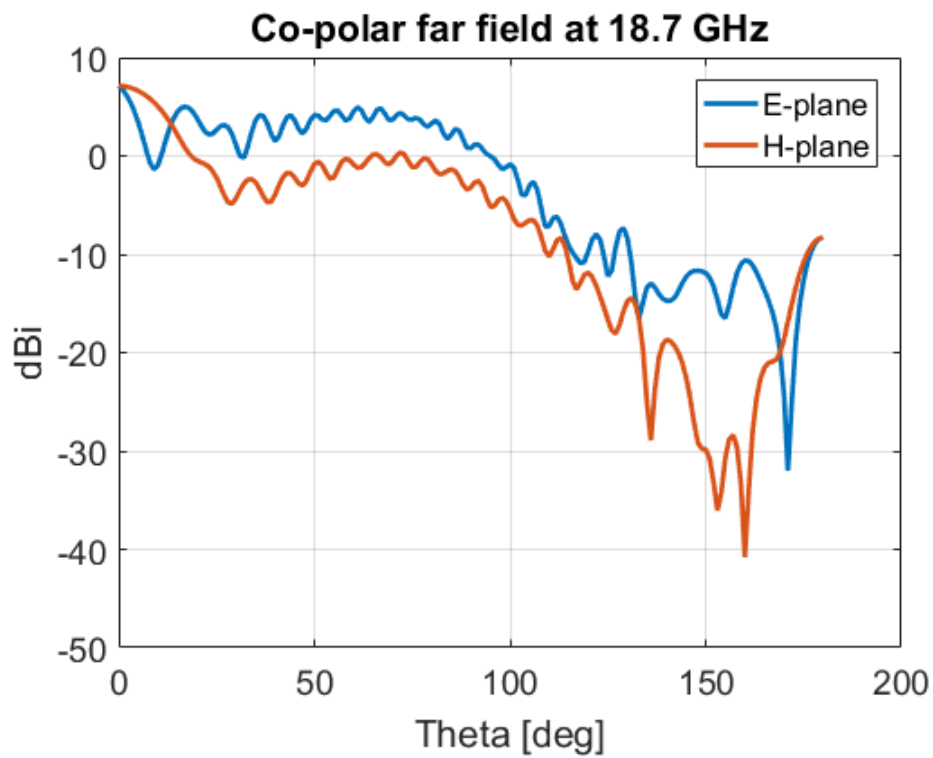


Figure 4.17: Farfield plot of the antenna feed with the sub reflector at 18.7 GHz. The angle is reversed, and 180 degrees is forward.

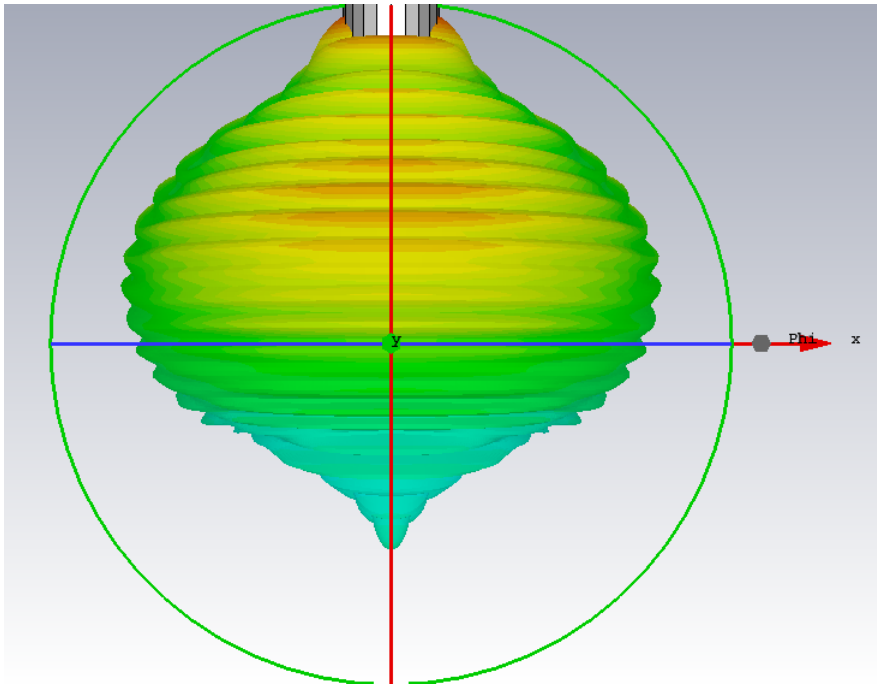


Figure 4.18: 3D Farfield plot of the H-plane of the antenna feed with the sub-reflector at 18.7 GHz

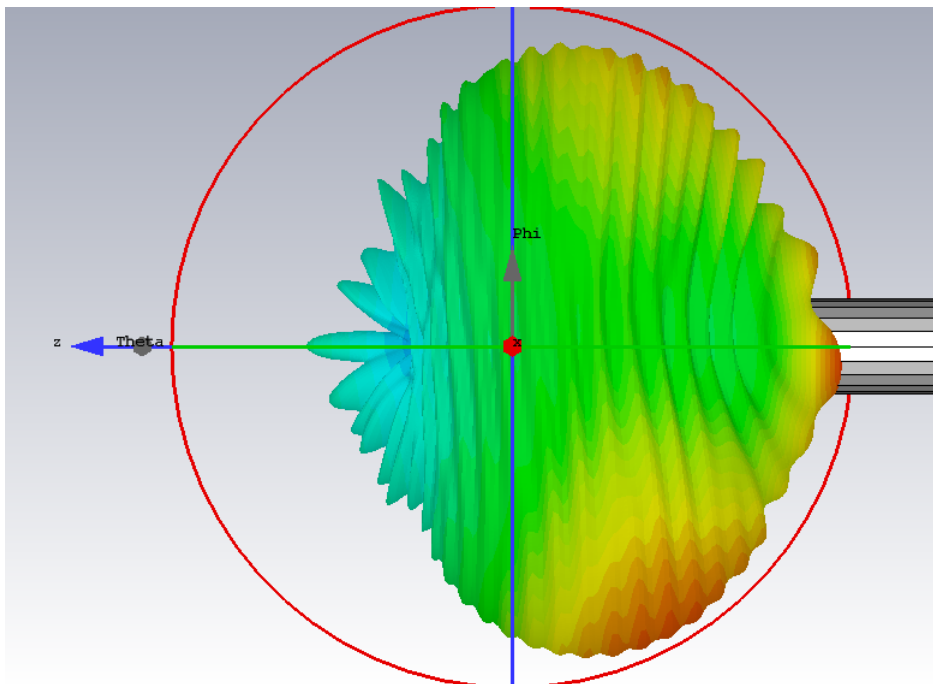


Figure 4.19: 3D Farfield plot of the E-plane of the antenna feed with the sub-reflector at 18.7 GHz

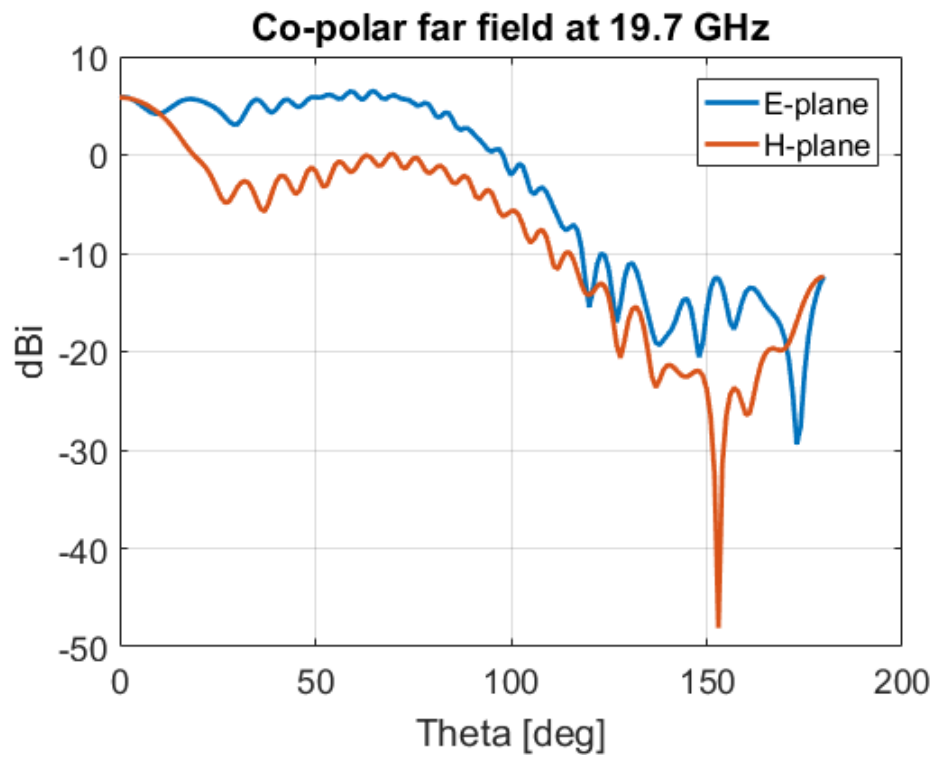


Figure 4.20: Farfield plot of the antenna feed with the sub reflector at 19.7 GHz. The angle is reversed, and 180 degrees is forward.

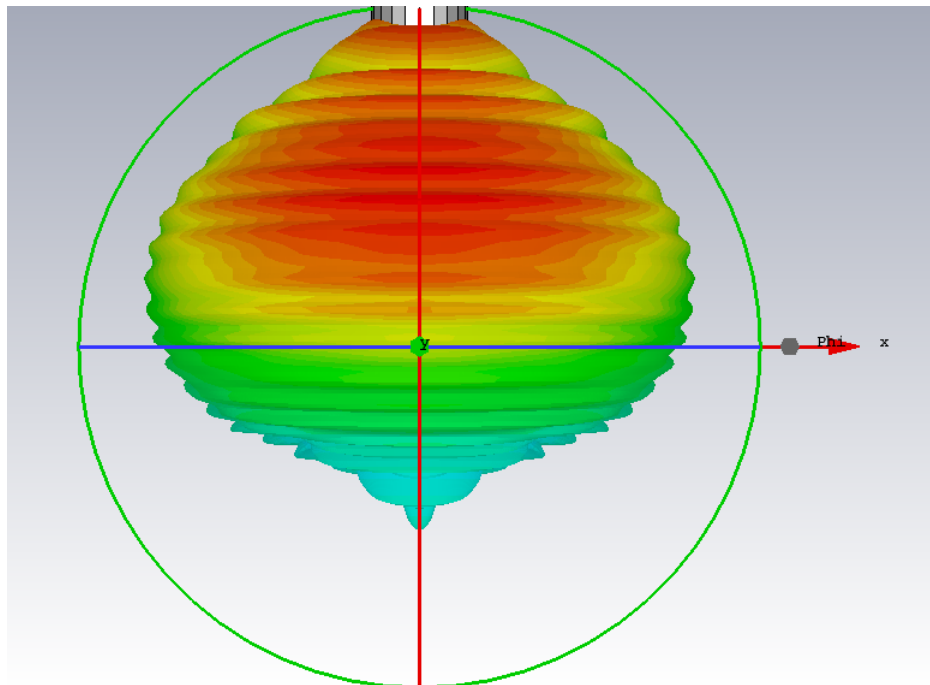


Figure 4.21: 3D Farfield plot of the H-plane of the antenna feed with the sub reflector at 19.7 GHz

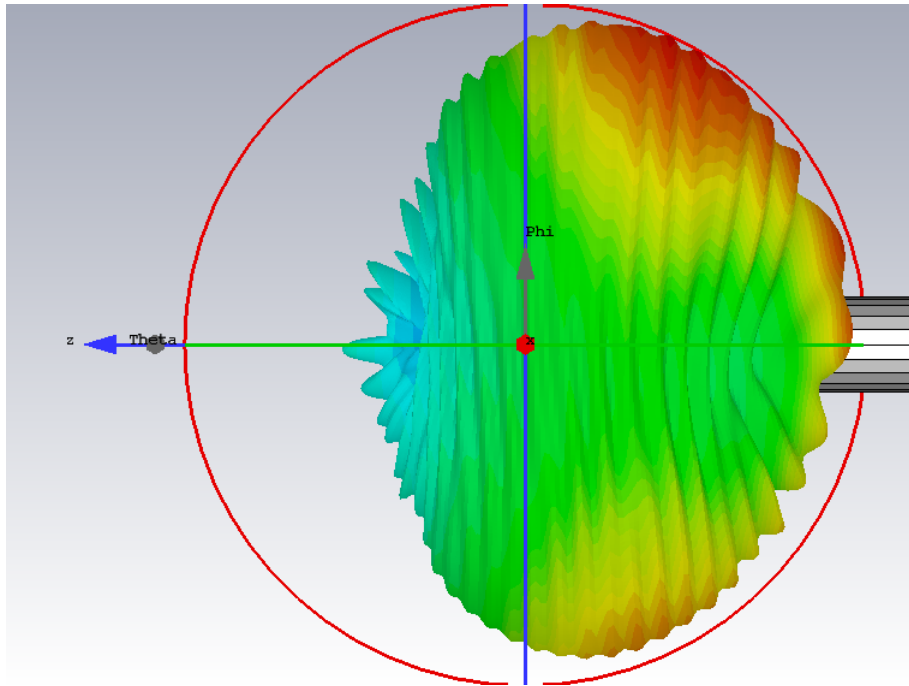


Figure 4.22: 3D Farfield plot of the E-plane of the antenna feed with the sub-reflector at 19.7 GHz

4.2 E-band

The same model was used for simulating at E-band. The results can be seen below.

The simulated reflection coefficient for the E-band port to port simulation can be seen in figure 4.23

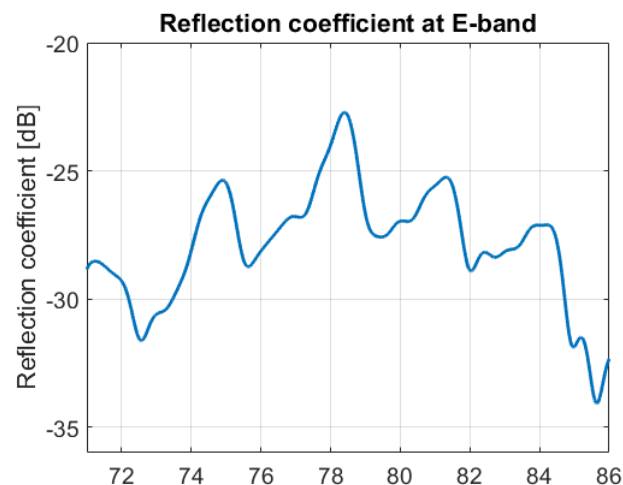


Figure 4.23: The simulated reflection coefficients for the E-band port to port simulation.

The simulated reflection coefficients when analyzing the feed as a horn antenna can

be seen in figure 4.24

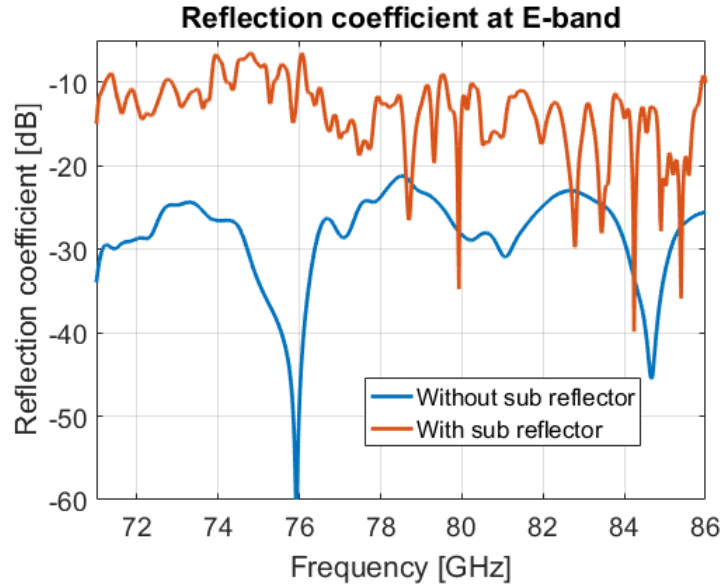


Figure 4.24: The simulated reflection coefficients for the E-band horn antenna simulation with and without sub reflector.

In table 4.2 the efficiencies can be found for the upper band.

freq (GHz)	e_{sp}	e_{ill}	e_{pol}	e_{ϕ}	e_{ap}
71	96%	89%	81%	52%	36%
78.5	96%	89%	74%	51%	32%
86	91%	88%	71%	26%	15%

Table 4.2: The efficiencies for the simulated antenna feed with sub reflector.

4.2.1 Farfield results

In the figures below the cartesian farfield plots and 3D-farfield plots can be seen for three different frequencies for the simulated structure without sub reflector.

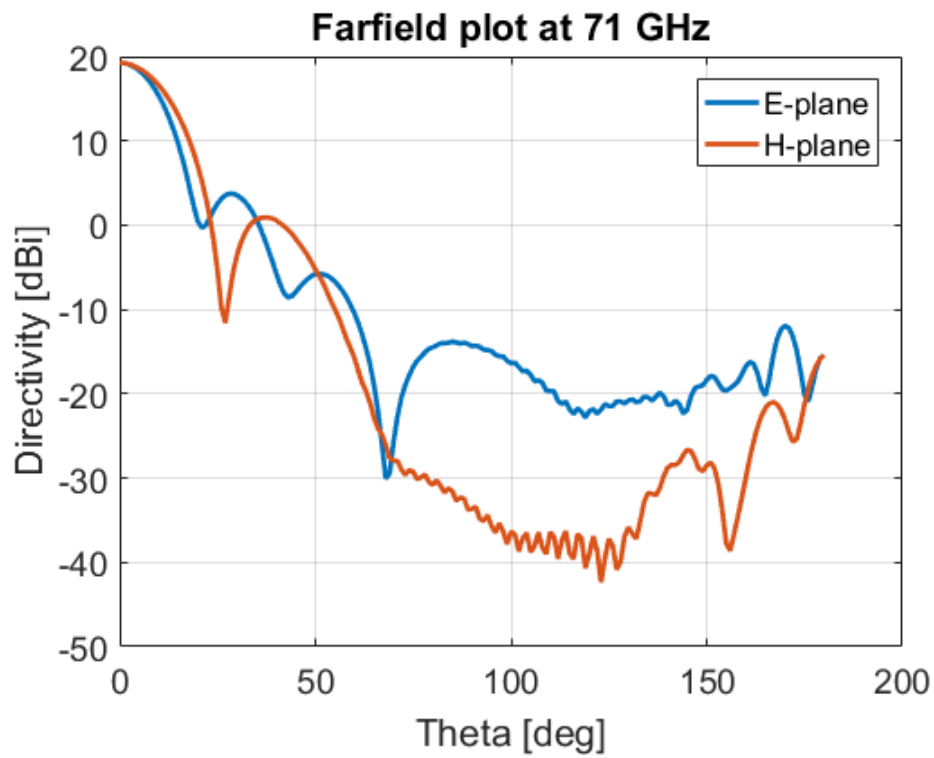


Figure 4.25: Farfield plot of the antenna feed at 71 GHz

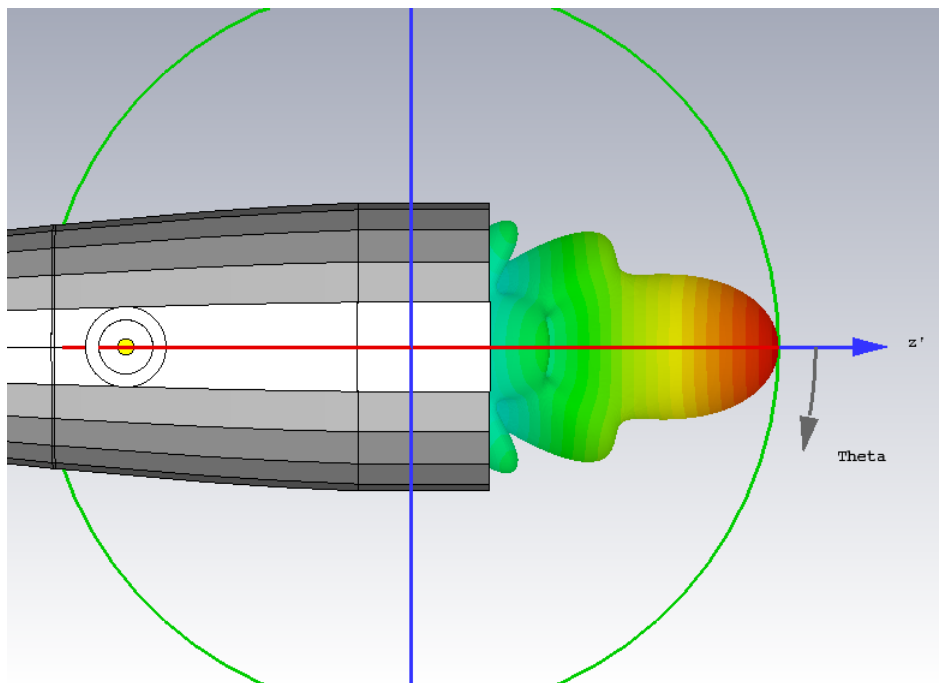


Figure 4.26: 3D Farfield plot of the E-plane of the antenna feed at 71 GHz

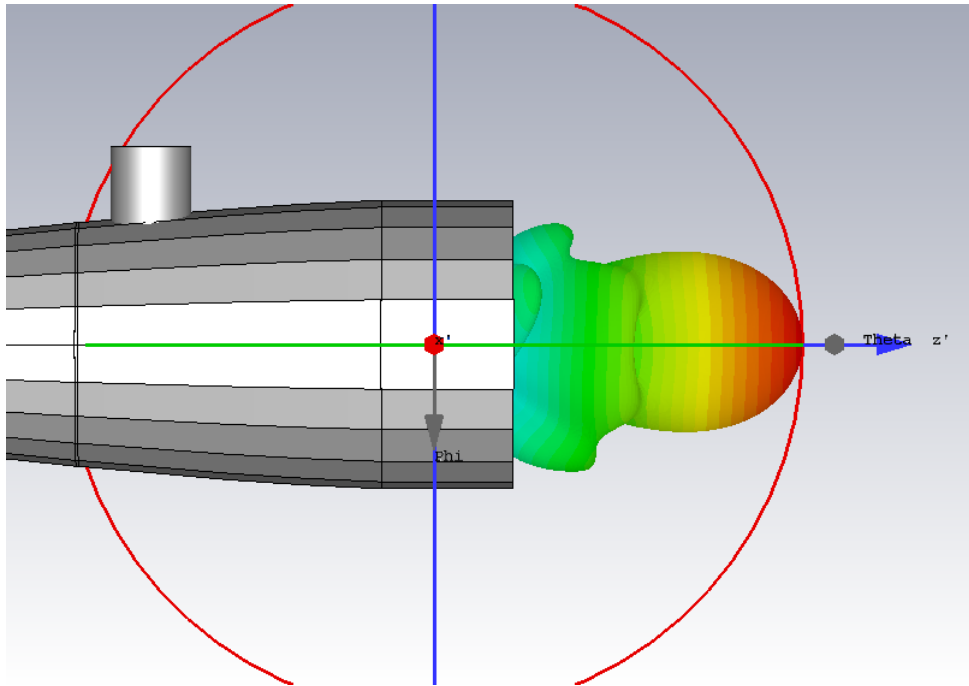


Figure 4.27: 3D Farfield plot of the H-plane of the antenna feed at 71 GHz

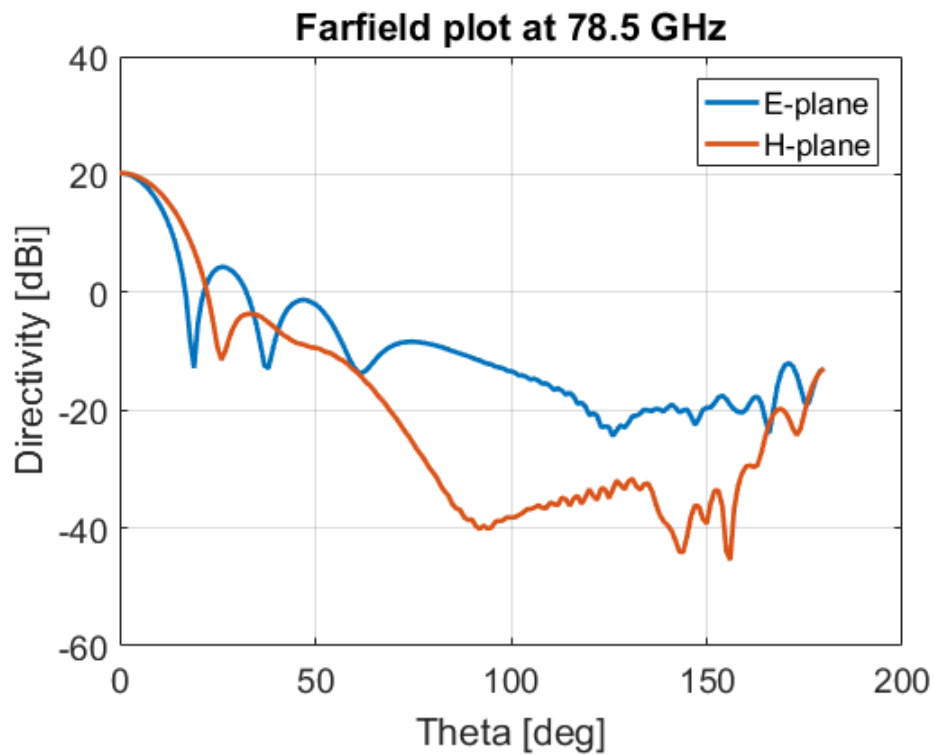


Figure 4.28: Farfield plot of the antenna feed at 78.5 GHz

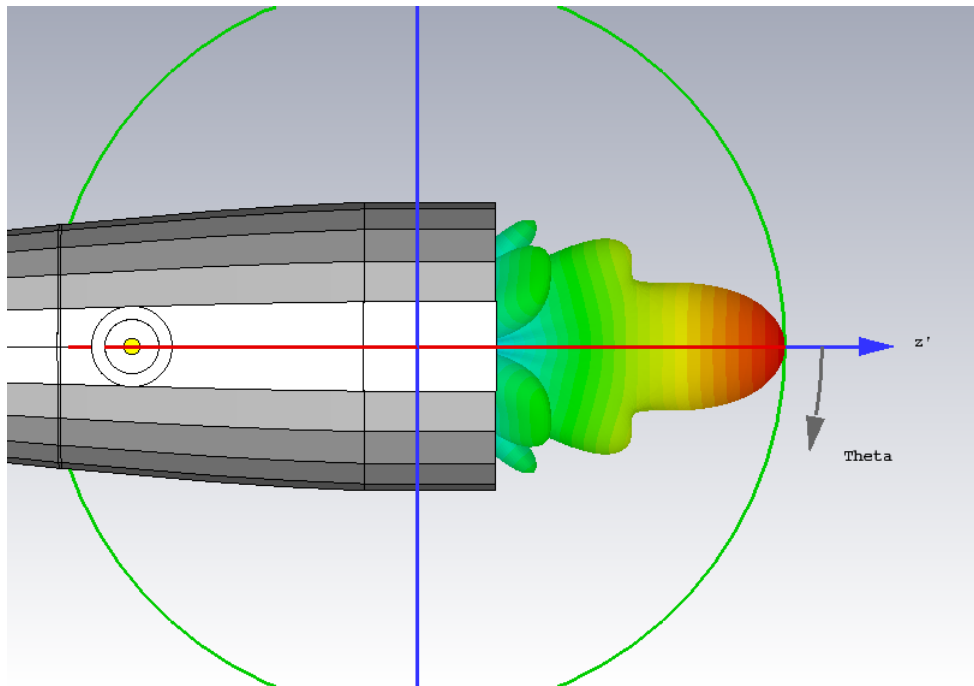


Figure 4.29: 3D Farfield plot of the E-plane of the antenna feed at 78.5 GHz

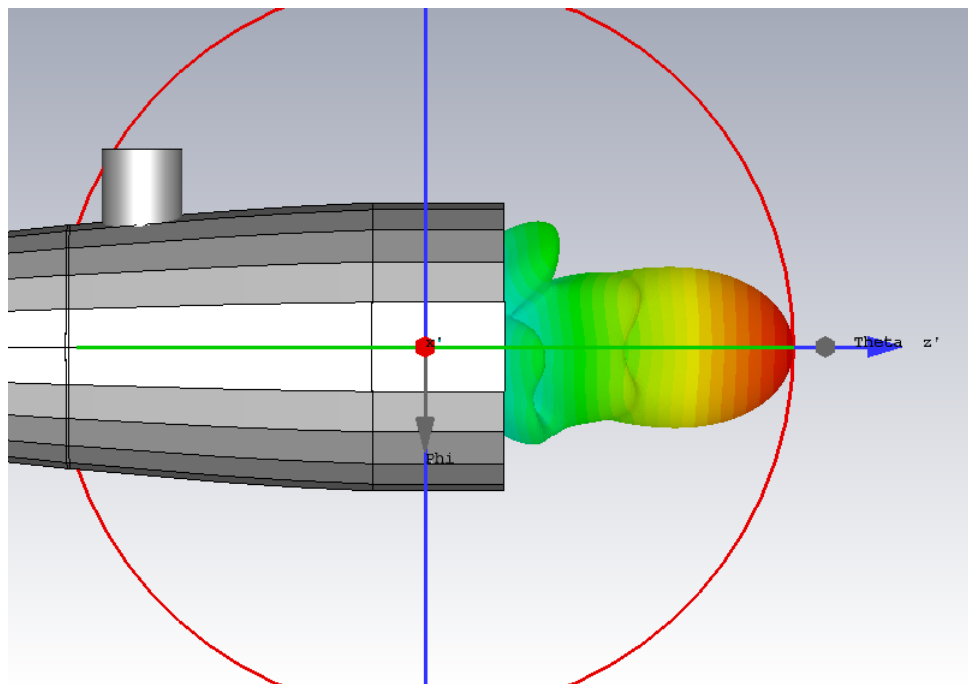


Figure 4.30: 3D Farfield plot of the H-plane of the antenna feed at 78.5 GHz

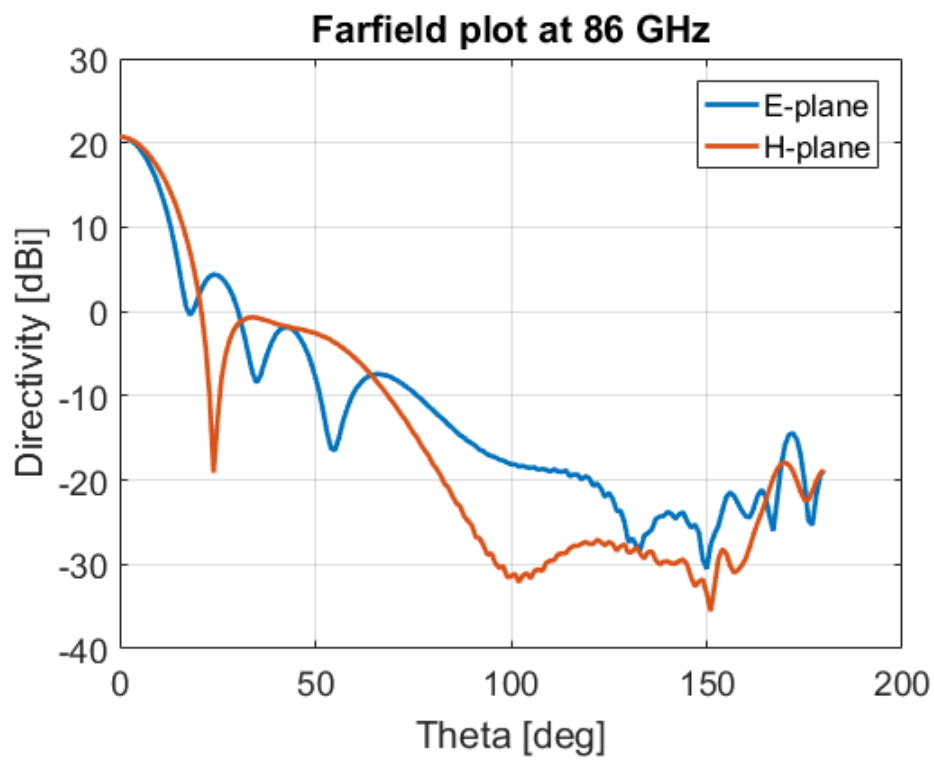


Figure 4.31: Farfield plot of the antenna feed at 86 GHz

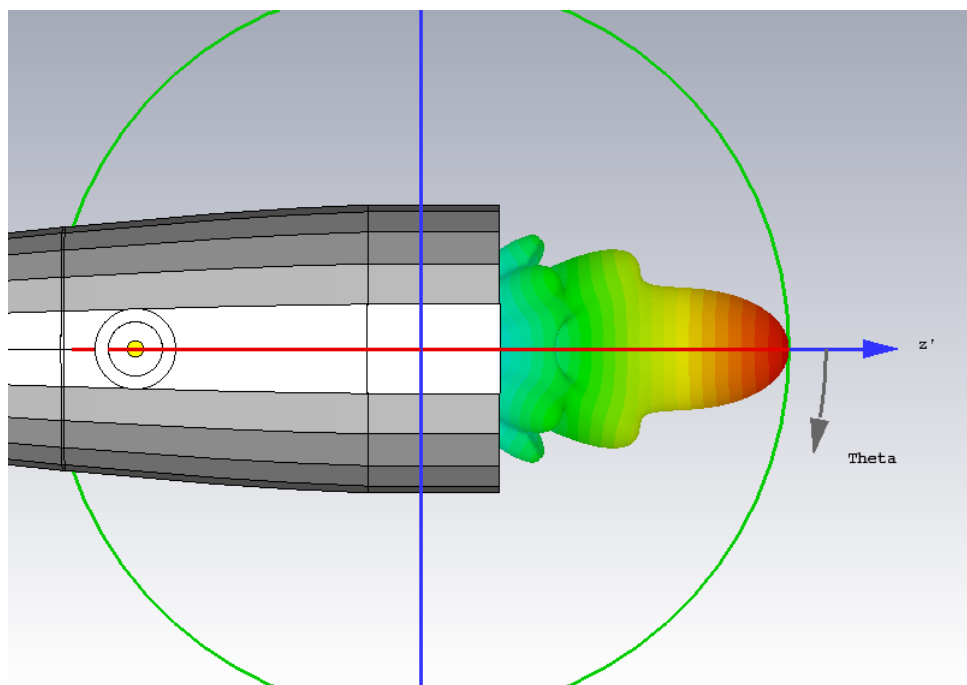


Figure 4.32: 3D Farfield plot of the E-plane of the antenna feed at 86 GHz

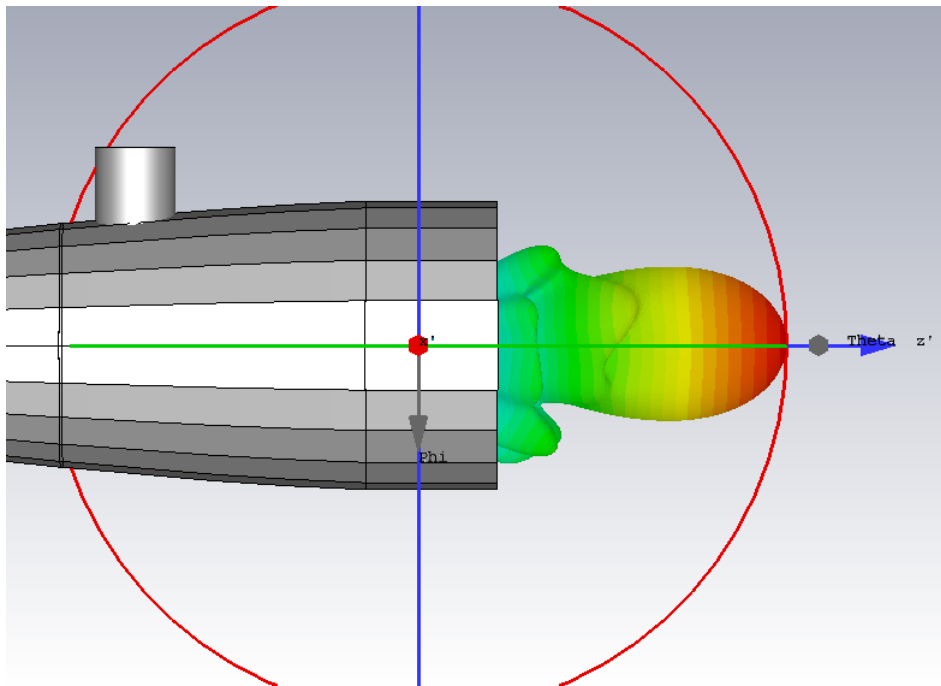


Figure 4.33: 3D Farfield plot of the H-plane of the antenna feed at 86 GHz

In the figures below the same simulations can be seen at E-band with the sub reflector.

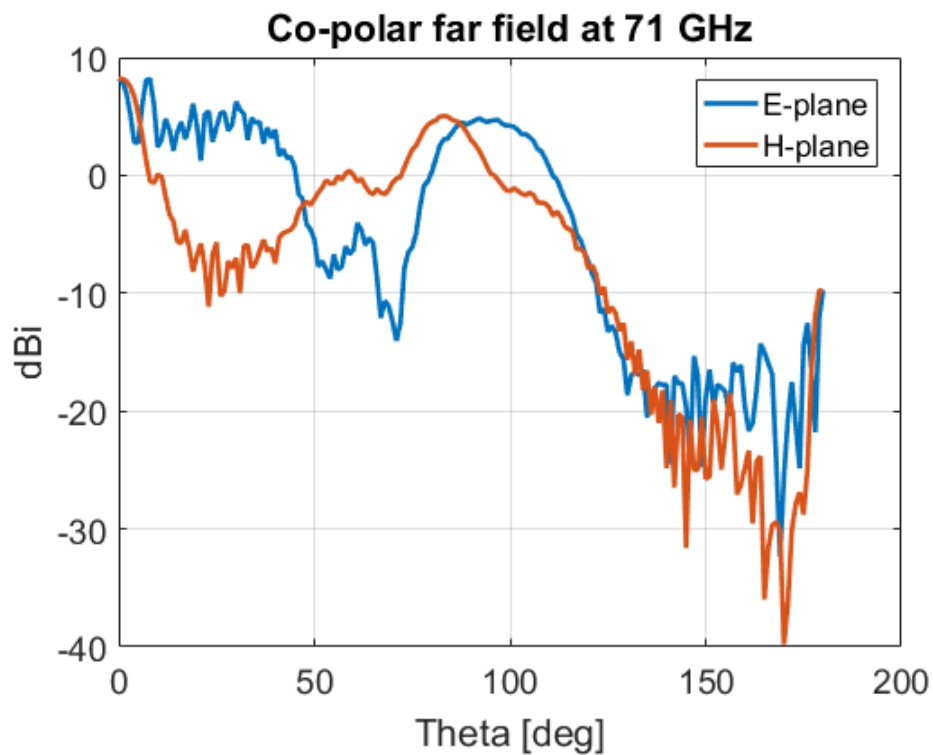


Figure 4.34: Farfield plot of the antenna feed with the sub reflector at 71 GHz. The angle is reversed, and 180 degrees is forward.

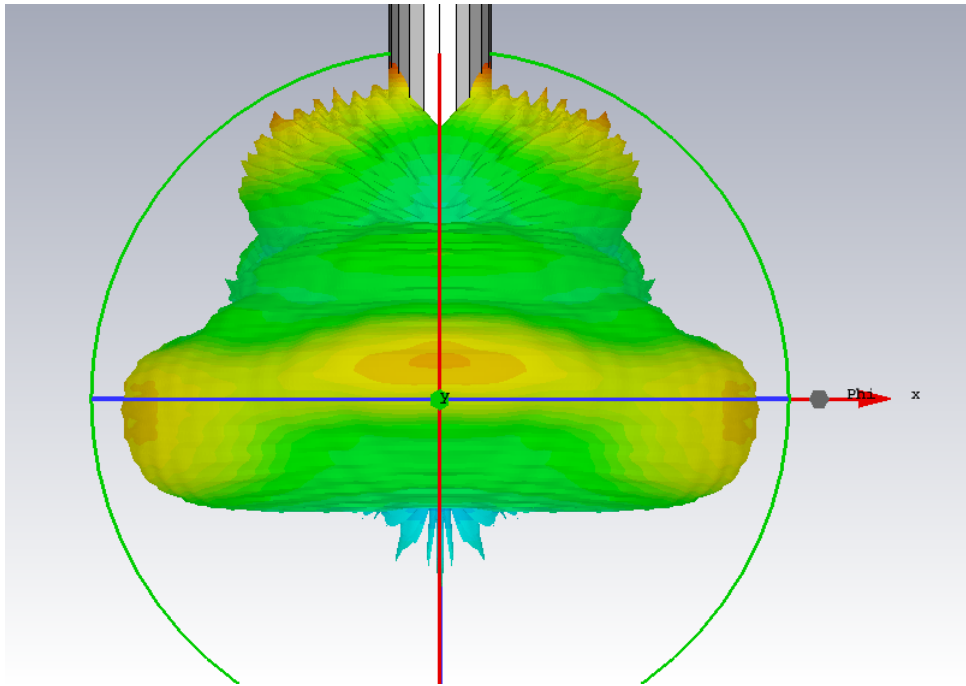


Figure 4.35: 3D Farfield plot of the E-plane of the antenna feed with the sub-reflector at 71 GHz

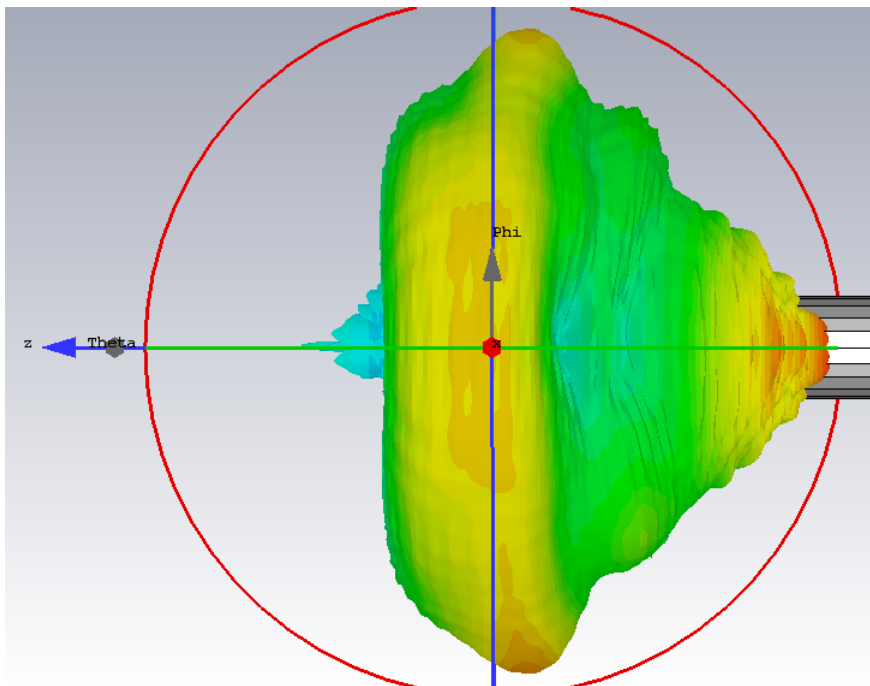


Figure 4.36: 3D Farfield plot of the H-plane of the antenna feed with the sub-reflector at 71 GHz

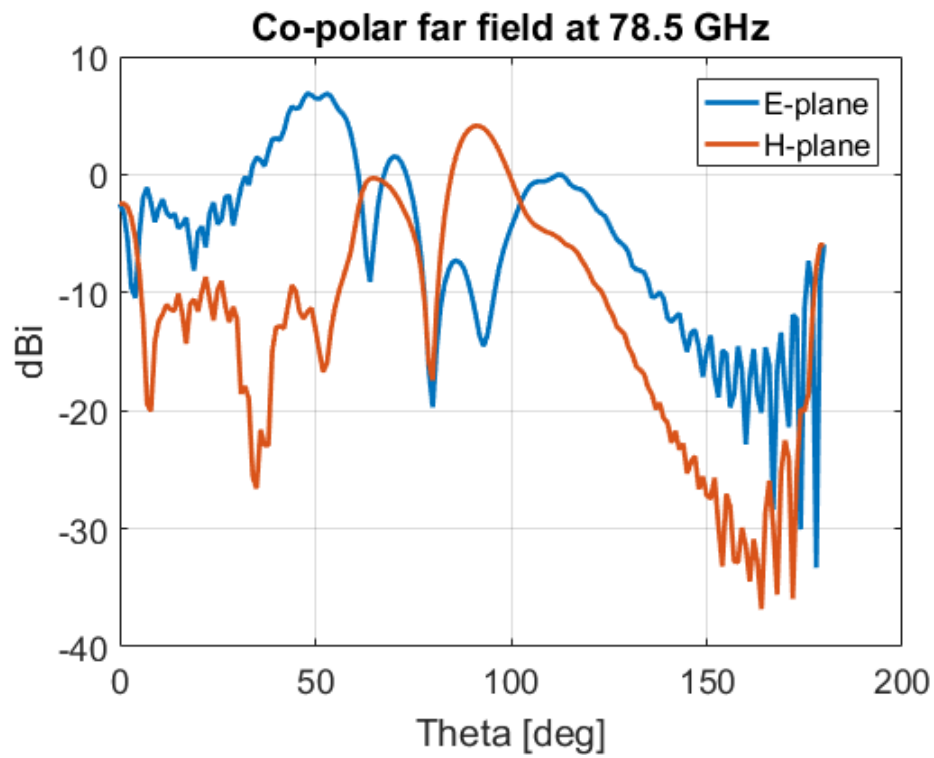


Figure 4.37: Farfield plot of the antenna feed with the sub reflector at 78.5 GHz. The angle is reversed, and 180 degrees is forward.

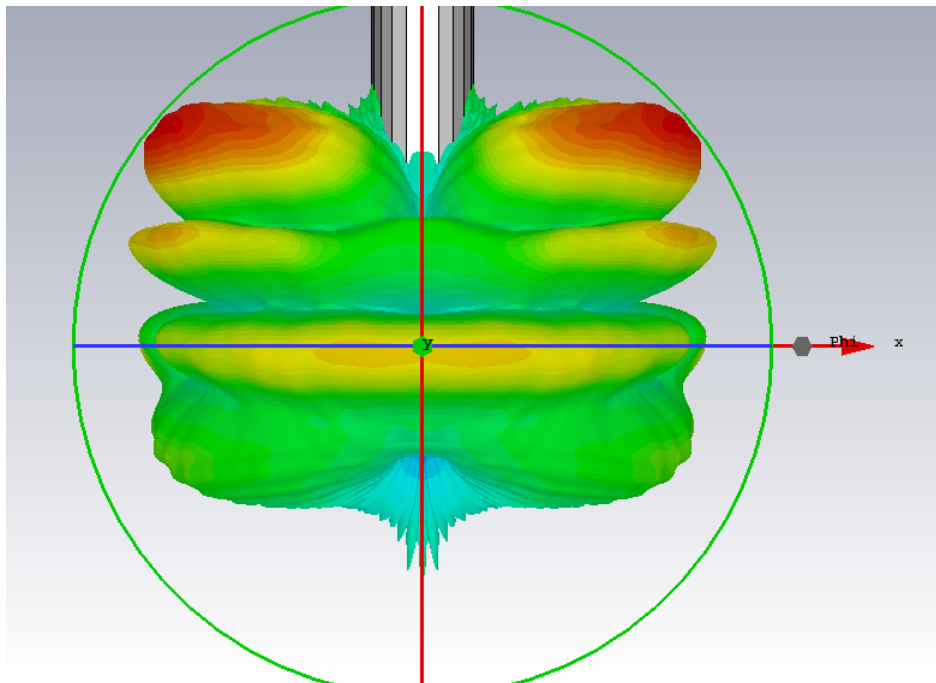


Figure 4.38: 3D Farfield plot of the E-plane of the antenna feed with the sub reflector at 78.5

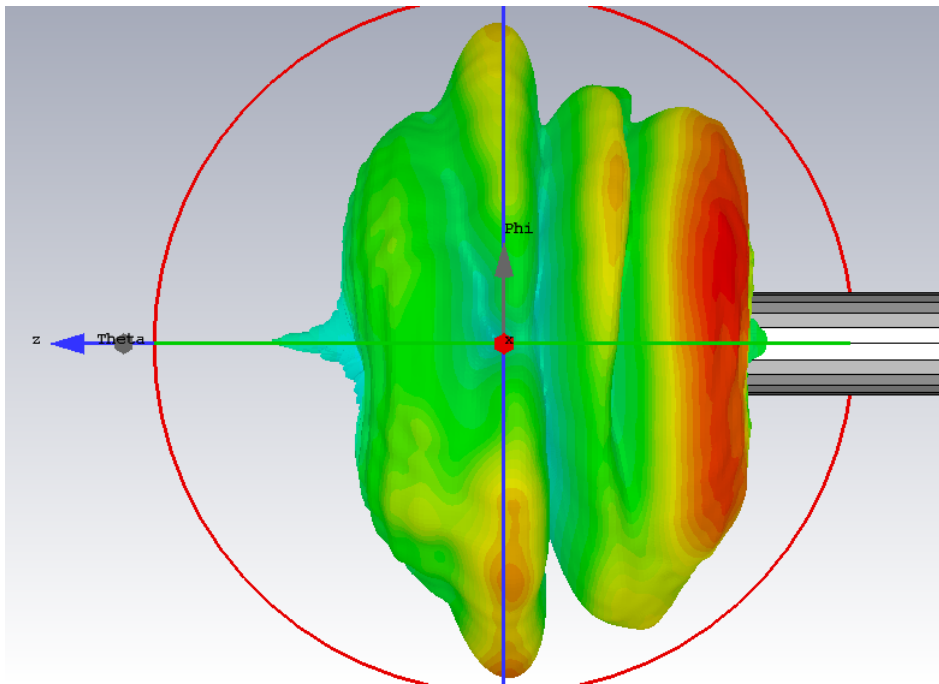


Figure 4.39: 3D Farfield plot of the H-plane of the antenna feed with the sub reflector at 78.5

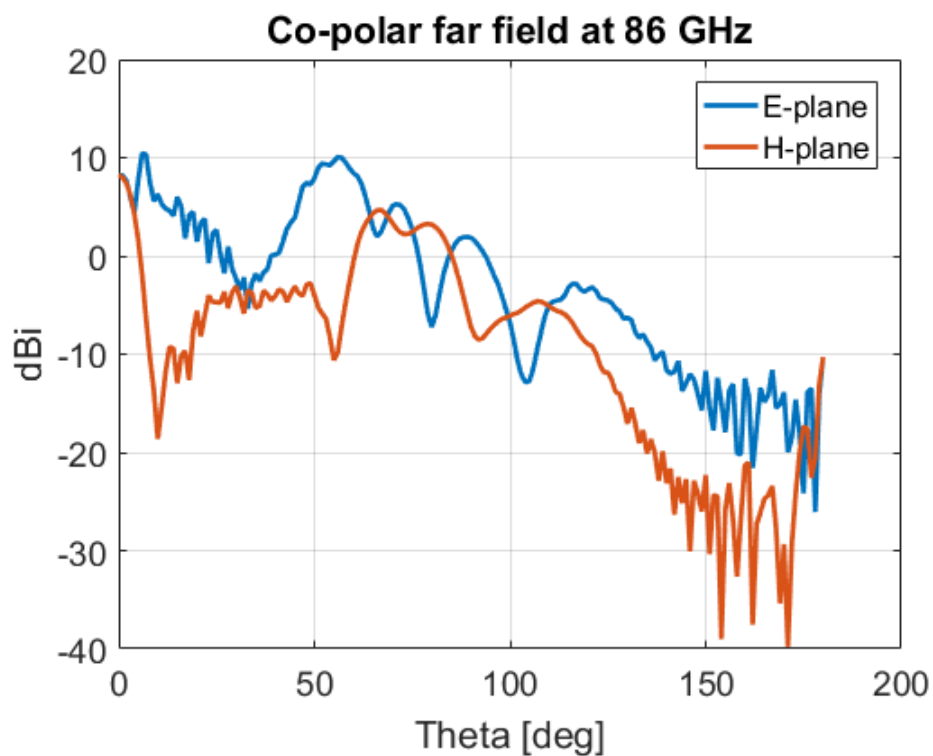


Figure 4.40: Farfield plot of the antenna feed with the sub reflector at 86 GHz. The angle is reversed, and 180 degrees is forward.

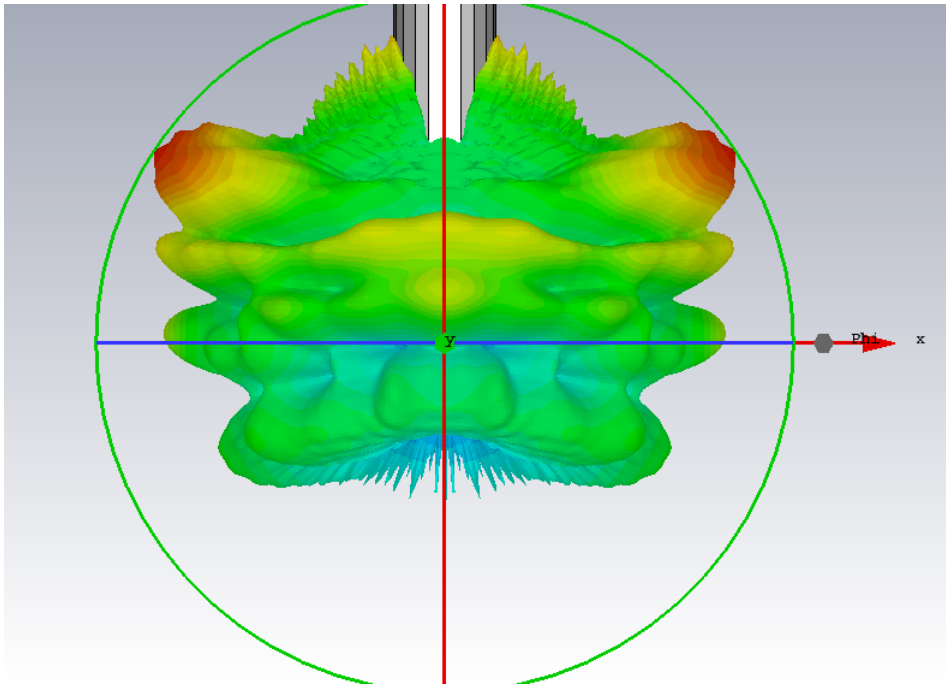


Figure 4.41: 3D Farfield plot of the E-plane of the antenna feed with the sub reflector at 86 GHz

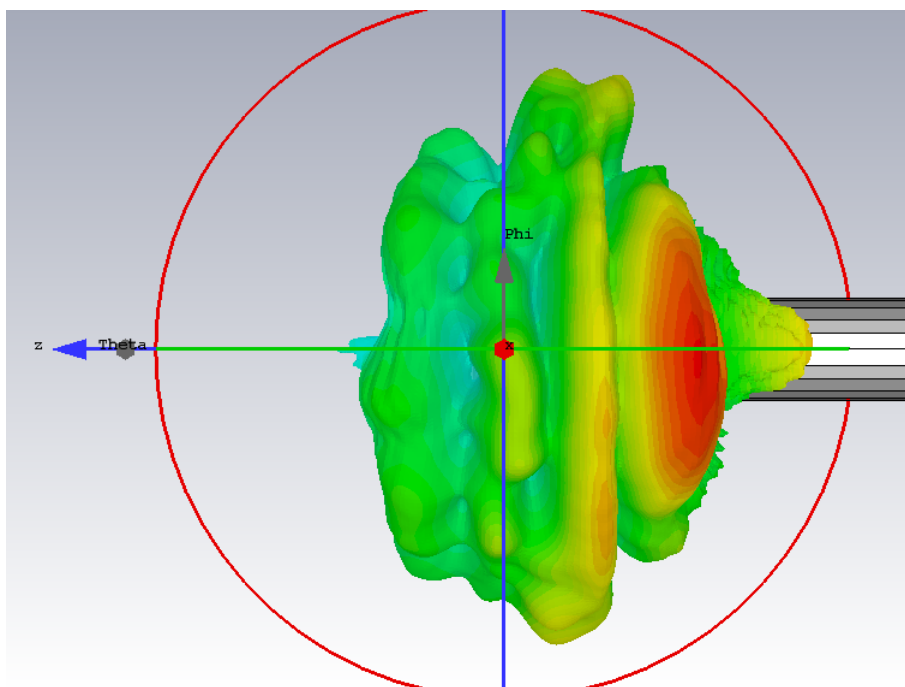


Figure 4.42: 3D Farfield plot of the E-plane of the antenna feed with the sub reflector at 86 GHz

5

Discussion and further work

5.1 Dual-band antenna feed

The main area which made this design difficult was the process of reducing the higher order modes prominent in the structure. The waveguide transition and initial ridge design excited many of the higher order modes which impacted the results negatively. This design process was highly focused on manufacturability as well, and was not a feasibility investigation of a dual-band dual-polarized feed in general. It would be interesting to investigate the feasibility of such an antenna feed, as it would more likely present the limitations and possibilities of the dual-band dual-polarized feed.

5.2 Ridge design

The ridge design approach is a very interesting solution which could be made for a dual-polarized setup. However, due to the limitations in coaxial cable and time the design was not continued with. I believe that with a customized coaxial feed setup the structure may perform well enough on both E-band and the 18 GHz-band. The limitations were that the required performance were not achieved on both bands simultaneously. The idea of using the cut-off properties of the waveguide as a reflecting wall is also interesting and should be investigated more thoroughly in order to understand the properties and how to efficiently design a ridge structure which can achieve the required results.

If this design is optimized enough it could most likely have a dual-band dual-polarized setup.

5.3 Pin structure design

The pin structure design was also an interesting approach for this project. It utilizes the polarization in a different way and is most likely more sensitive to polarization errors than the previous design, as this would then be affected by the pins as they are no longer orthogonal to the field. This structure also performed good on both bands, and was the desired structure for manufacturing. The limitation as mentioned previously however, is that it is most likely not possible to re-design to work for dual-polarized setups, and may thus not be as interesting to purchase from a buyers point of view.

5.4 Results

The results were decided to be good enough for the manufacturing of a prototype which is to be measured upon. These measurements might also give information about the reliability of the simulation of the pin structure design, and its impact by tolerances. It will also, to some extent, reveal the impact on E-band in reality. This will be key for future development of the antenna feed and to understand the feasibility of the pin structure design.

Overall, looking at the S-parameter simulations (i.e. reflection and transmission) the design is usable. However, looking at the efficiencies they differ highly between the both frequency bands. This is discussed below.

5.4.1 Efficiencies

The aperture efficiency for the both bands differ by more than 30%. The efficiencies that differ the most are the polarization more prominently, the phase efficiencies. This can be explained by the fact that the phase along the waveguide section is not constant as is wanted. The phase changes with the radial distance from the center of the structure, which is most likely due to the size of the waveguide structure and higher order modes being excited throughout the structure. Especially at the interface between the sub-reflector and waveguide feed since there is a distinct change in structural layout within the waveguide. It would be beneficial to simulate with an optimized sub-reflector structure for this antenna feed to investigate the impact on the phase efficiencies.

5.5 Future work

For future works there are two main areas that should be investigated more thoroughly. The ridge design and OMT.

For the ridge design there were promising results for either 18 GHz or E-band. If there is a possibility to customize a coaxial cable the performance at the lower band may be improved and be good for both bands. I believe that the performance will be good enough for both bands if the design is more optimizable.

OMT is a well used structural layout for dual-polarized setups. As no investigations were made in this area it could be of interest to do a rigorous analysis of how well it may perform in a dual-band setup as well, and investigate the performance relative to a ridge design and pin structure design.

It would also be interesting to optimize the sub reflector and investigate the results, as when it was introduced the performance of the system was reduced by a large margin.

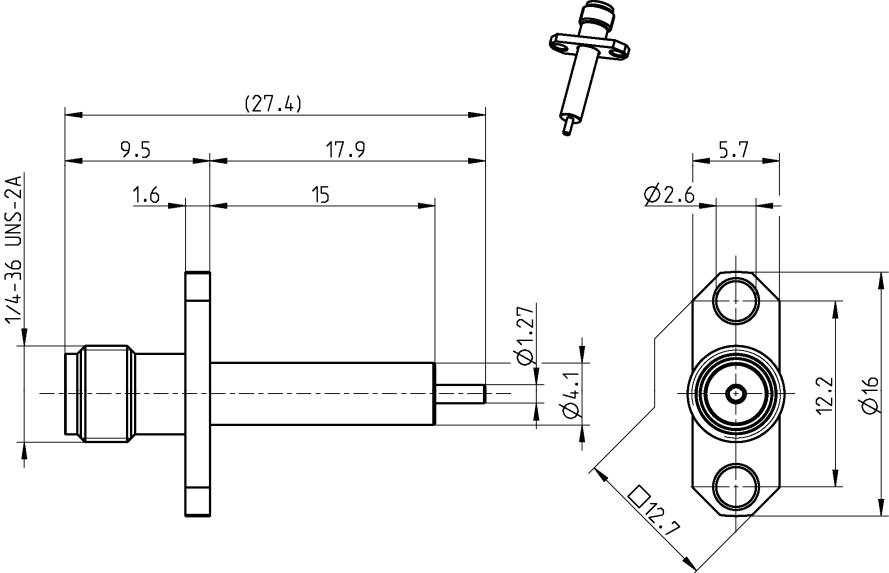
Bibliography

- [1] M. F. Y. Musthofa, A. Munir, "Design of Rectangular to Circular Waveguide Converter for S-Band Frequency", in 2011 International Conference on Electrical Engineering and Informatics, Bandung, Indonesia, 2011, [Online]. Available: <https://ieeexplore.ieee.org/document/6021720/>, acquired 2018-04-16.
- [2] D. M. Pozar, Microwave Engineering, fourth edition, USA: John Wiley & Sons, Inc., 2012.
- [3] P. S. Kildal, Foundations of Antenna Engineering: A Unified Approach for Line-Of-Sight and Multipath. Gothenburg, Sweden: Kildal Antenn AB, 2015.
- [4] P.S. Kildal, "The hat feed: a dual-mode rear-radiating wave-guide antenna having low cross-polarization," *IEEE Trans. Antennas Propag.*, 1987, 35, (9), pp. 1010–1016
- [5] W. Wei, J. Yang, T. Ostling, and T. Schafer, "A new hat feed for reflector antennas realized without dielectrics for reducing manufacturing cost and improving reflection coefficient," *IET Microwaves Antennas Propag.*, vol. 5, no. 7, pp. 837–843, Jul. 2011
- [6] E. G. Geterud, J. Yang, T. Ostling, and P. Bergmark, "Design and optimization of a compact wideband hat-fed reflector antenna for satellite communications", *IEEE Trans. Antenna Propagat.*, vol. 61, no. 1, pp.125–133, 2013
- [7] H. Prautzsch, W. Boehm and M. Paluszny, Bézier and B-Spline Techniques, Berlin, Germany: Springer-Verlag Berlin Heidelberg, 2002
- [8] S.J. Skinner and G.L. James, "Wide-Band Orthomode Transducer", *IEEE Transactions on microwave theory and techniques*, vol. 39, No. 2, ss. 294-300, feb. 1991.
- [9] J. L. Yu, C. J. Jin, Y. Cao and H. S. Chen, "Broad-band orthomode transducers," *2008 International Conference on Microwave and Millimeter Wave Technology*, Nanjing, 2008, pp. 320-322.
- [10] J. Uher, J. Bornemann and U. Rosenberg, *Waveguide Components for Antenna Feed Systems: Theory and CAD*, Norwood, MA, USA: Artech House Inc., 1993
- [11] R. Dey, S.B. Chakrabarty, and R. Jyoti, "Analysis of a coaxial probe-fed circular waveguide", *Microwave and optical technology letters*, vol. 55, no. 11, ss. 2652-2656
- [12] D. I. L. D. Villiers, P. Meyer and K. D. Palmer, "Broadband offset quad-ridged waveguide orthomode transducer", in *Electronics Letters*, vol. 45, no. 1, pp. 60-62, January 1 2009.
- [13] A. Akgiray, S. Weinreb and W. Imbriale, "Design and measurements of dual-polarized wideband constant-beamwidth quadruple-ridged flared horn", 2011

- IEEE International Symposium on Antennas and Propagation (APSURSI), Spokane, WA, 2011, pp. 1135-1138.
- [14] J. Shi, S. Weinreb, W. Zhong, X. Yin and M. Yang, "*Quadruple-Ridged Flared Horn Operating From 8 to 50 GHz*", in IEEE Transactions on Antennas and Propagation, vol. 65, no. 12, pp. 7322-7327, Dec. 2017.

A

Appendix 1

TECHNICAL DATA SHEET	Rosenberger	
SMA	PANEL JACK STRAIGHT TERMINAL	32K722-500E3
		
All dimensions are in mm; tolerances according to ISO 2768 m-H		
Interface		
According to IEC 60169-15; EN 122110; MIL-STD-348		
Documents		
Panel piercing B 55a		
Material and plating		
Connector parts		
Center contact	Material Beryllium copper	Plating Gold, min. 1.27 µm, over chemical nickel
Outer contact	Stainless steel	Gold, min. 0.8 µm, over nickel
Dielectric	PTFE	
RF_35/12.04/3.0	Rosenberger Hochfrequenztechnik GmbH & Co. KG P.O.Box 1260 D-84526 Tittmoning Germany www.rosenberger.de	Tel.: +49 8684 18-0 email: info@rosenberger.de
II		Page 1 / 2